Journal of Medicinal Chemistry

Article

pubs.acs.org/jmc

Alkyl Substituted 2′-Benzoylpyridine Thiosemicarbazone Chelators with Potent and Selective Anti-Neoplastic Activity: Novel Ligands that Limit Methemoglobin Formation

Christian Stefani,[†] Patric J. Jansson,[†] Elaine Gutierrez,[†] Paul V. Bernhardt,[‡] Des R. Richardson,[†,*] and Danuta S. Kalinowski*[,†]

[†]Iron Metabolism and Chelation Program, Department of Pathology, University of Sydney, Sydney, New South Wales 2006, Australia

[‡]Centre for Metals in Biology, School of Chemistry and Molecular Biosciences, University of Queensland, Brisbane, Qld 4072, Australia

Supporting Information

ABSTRACT: Thiosemicarbazone chelators, including the 2′-benzoylpyridine thiosemicarbazones (BpT) class, show marked potential as anticancer agents. Importantly, 3-aminopyridine-2-carboxaldehyde thiosemicarbazone (3-AP) has been investigated in >20 phase I and II clinical trials. However, side effects associated with 3-AP administration include methemoglobinemia. Considering this problem, novel BpT analogues were designed bearing hydrophobic, electron-donating substituents at the *para* position of the phenyl group (RBpT). Their $Fe^{III/II}$ redox potentials were all within the range accessible to cellular oxidants and reductants, suggesting they can redox cycle. These RBpT ligands exhibited potent and selective antiproliferative activity, which was comparable or exceeded their BpT counterparts. Major findings include that methemoglobin formation mediated by the lipophilic *t*-BuBpT series was significantly ($p < 0.05-0.001$) decreased in comparison to 3-AP in intact red blood cells and were generally comparable to the control. These data indicate the *t*-BuBpT ligands may minimize methemoglobinemia, which is a marked advantage over 3-AP and other potent thiosemicarbazones.

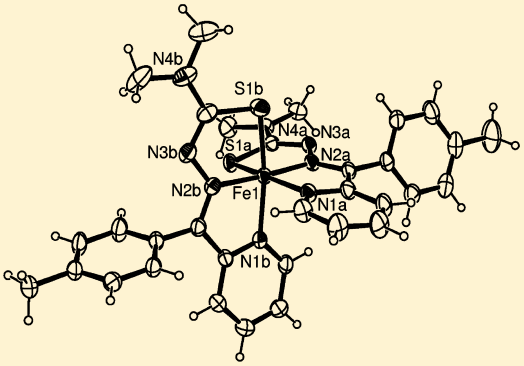

INTRODUCTION

Iron (Fe) is essential for life and catalyzes key reactions involved in metabolism, respiration, oxygen transport, and DNA synthesis.[1] Rapidly growing neoplastic cells, such as neuroblastoma[2] and leukemia,[3] have particularly high demands for iron.[4] This increased requirement for iron is reflected in the increased expression of the transferrin receptor 1 (TfR1) in cancer cells, which is involved in the cellular uptake of iron from transferrin (Tf).[5] In addition, cancer cells express higher levels of the iron-containing enzyme, ribonucleotide reductase (RR),[6] which is pivotal in the rate-limiting step of DNA synthesis that can be targeted by iron chelators.[7,8] These characteristics suggest that iron represents a potential therapeutic target for cancer treatment.

Many in vitro and in vivo studies and clinical trials have demonstrated that iron chelators are effective antiproliferative agents.[9−18] It has been observed that the iron chelator, desferrioxamine (DFO; Figure 1A), can modestly inhibit tumor growth both in experimental models and in clinical trials.[9,13] Iron chelators are able to sequester iron from biological systems, and hence are able to inhibit the activity of iron-requiring proteins, including RR.[7,8,11] Additionally, iron depletion also impedes cell cycle progression (G_1 to S phase) and alters the expression of a number of molecules involved in growth and metastasis suppression.[19−22]

Encouraged by the modest results obtained with traditional iron chelators, a variety of novel ligands with antiproliferative activity have been identified, including 2-hydroxy-1-napthaldehyde isonicotinoyl hydrazone (NIH; Figure 1A),[23,24] pyridoxal isonicotinoyl hydrazone (PIH; Figure 1A),[23−25] tachpyridine (Figure 1A),[16] 3-aminopyridine-2-carboxaldehyde thiosemicarbazone (3-AP),[26,27] and di-2-pyridylketone 4,4-dimethyl-3-thiosemicarbazone (Dp44mT; Figure 1A).[28,29] In fact, 3-AP has been investigated in over 20 phase I and phase II clinical trials in a variety of advanced cancers.[30−32] Unfortunately, the side effects associated with 3-AP administration include hypoxia and methemoglobinemia (resulting from the oxidation of oxyhemoglobin (oxyHb; Fe^{II}) to methemoglobin (metHb; Fe^{III})), which limits its clinical utility.[33−35] We previously demonstrated that the formation of the redox active 3-AP iron complex was essential in metHb generation.[36] The detrimental side effects associated with 3-AP administration are a major concern in patients with compromised cardiopulmonary

Received: November 16, 2012
Published: December 31, 2012

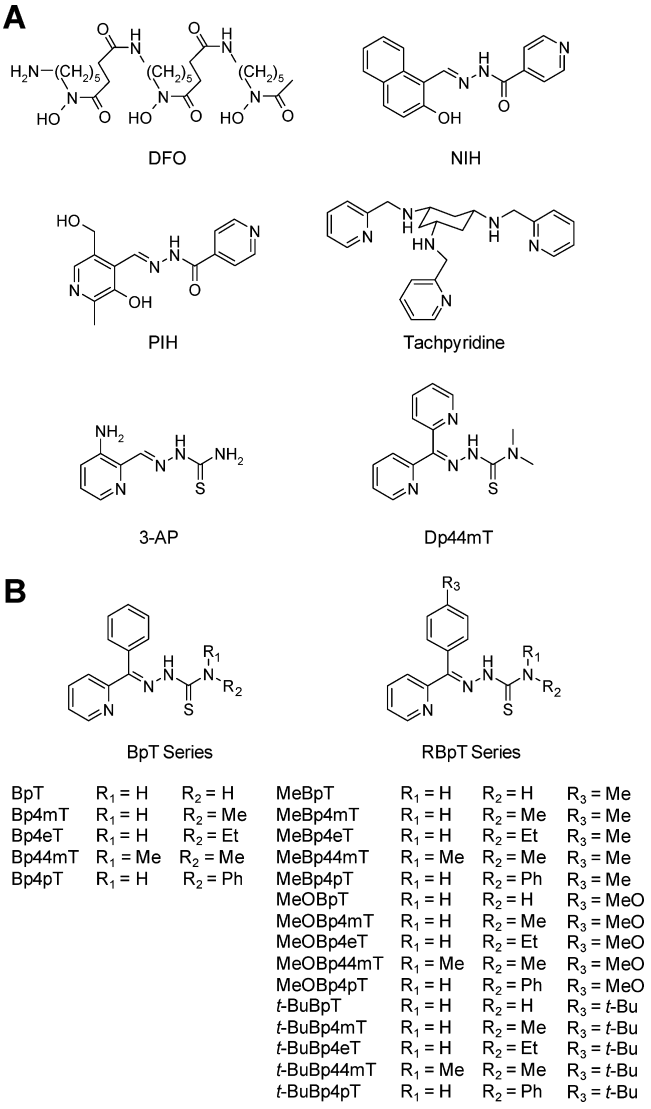

BpT	R_1 = H	R_2 = H	MeBpT	R_1 = H	R_2 = H	R_3 = Me
Bp4mT	R_1 = H	R_2 = Me	MeBp4mT	R_1 = H	R_2 = Me	R_3 = Me
Bp4eT	R_1 = H	R_2 = Et	MeBp4eT	R_1 = H	R_2 = Et	R_3 = Me
Bp44mT	R_1 = Me	R_2 = Me	MeBp44mT	R_1 = Me	R_2 = Me	R_3 = Me
Bp4pT	R_1 = H	R_2 = Ph	MeBp4pT	R_1 = H	R_2 = Ph	R_3 = Me
			MeOBpT	R_1 = H	R_2 = H	R_3 = MeO
			MeOBp4mT	R_1 = H	R_2 = Me	R_3 = MeO
			MeOBp4eT	R_1 = H	R_2 = Et	R_3 = MeO
			MeOBp44mT	R_1 = Me	R_2 = Me	R_3 = MeO
			MeOBp4pT	R_1 = H	R_2 = Ph	R_3 = MeO
			t-BuBpT	R_1 = H	R_2 = H	R_3 = *t*-Bu
			t-BuBp4mT	R_1 = H	R_2 = Me	R_3 = *t*-Bu
			t-BuBp4eT	R_1 = H	R_2 = Et	R_3 = *t*-Bu
			t-BuBp44mT	R_1 = Me	R_2 = Me	R_3 = *t*-Bu
			t-BuBp4pT	R_1 = H	R_2 = Ph	R_3 = *t*-Bu

Figure 1. (A) Chemical structures of the iron chelators, desferrioxamine (DFO), 2-hydroxy-1-naphthaldehyde isonicotinoyl hydrazone (NIH), pyridoxal isonicotinoyl hydrazone (PIH), tachpyridine, 3-aminopyridine-2-carboxaldehyde thiosemicarbazone (3-AP), and di-2-pyridylketone 4,4-dimethyl-3-thiosemicarbazone (Dp44mT). (B) Chemical structures of members of the 2′-benzoylpyridine thiosemicarbazone (BpT) series of ligands and their *p*-alkyl substituted counterparts (RBpT).

function and is a critical aspect to consider in the design of novel iron chelators as anticancer agents.

We previously reported the synthesis of the di-2-pyridylketone thiosemicarbazone (DpT) class of chelators, in particular Dp44mT (Figure 1A), which demonstrated potent and selective antitumor activity in vitro and in vivo against a variety of tumor models in mice.[28,29,37] However, cardiac fibrosis was evident at high, nonoptimal doses.[37] The electrochemistry of the iron complex of Dp44mT showed facile interconversion between the Fe^{II} and Fe^{III} states within the range accessible to cellular oxidants and reductants (~+100 to +250 mV vs normal hydrogen electrode (NHE)).[28] Electron spin resonance trapping also suggested that $Fe(Dp44mT)_2$ can reduce H_2O_2, generating reactive oxygen species (ROS) such as the hydroxyl radicals ($HO^{\bullet}$)[38] and is an important mechanism in its potent antiproliferative activity.[28] Interestingly, earlier studies have demonstrated that this class of thiosemicarbazone form highly stable Fe^{III} complexes and are likely to be highly competitive for Fe^{III} in vivo over other divalent metals, including Mn^{II}, Co^{II}, Ni^{II}, Zn^{II}, and Cu^{II}.[39] In fact, their Mn^{II}, Co^{II}, Ni^{II}, Zn^{II}, and Cu^{II} complexes are able to undergo transmetalation in the presence of Fe^{II}.[39] However, the formation constant of the Fe^{II} complexes could not be determined due to inability of ligands (e.g., nitrilotriacetate, ethylenediaminetetraacetic acid, and diethylene triamine pentaacetic acid) to effectively compete with the Fe-coordinated thiosemicarbazone.[39]

The development of the DpT class of ligands was followed by the 2′-benzoylpyridine thiosemicarbazone (BpT; Figure 1B) series, in which the noncoordinating 2-pyridyl moiety of the DpT analogues was substituted with a phenyl ring.[40] Recent studies in vivo using nude mice bearing a human DMS-53 lung cancer xenograft showed that the BpT series analogue, 2′-benzoylpyridine 4,4-dimethyl-3-thiosemicarbazone (Bp44mT), can be administered intravenously or orally with potent antitumor efficacy and no cardiotoxicity.[41] Electrochemistry of their iron complexes revealed lower $Fe^{III/II}$ redox potentials (+99 to +180 mV vs NHE) than their analogous DpT homologues, and it was shown that the BpT Fe complexes could effectively oxidize ascorbate.[40] The lower electron-withdrawing property of the phenyl moiety relative to the pyridyl ring probably contributes to the lowered $Fe^{III/II}$ redox potentials.[40]

In this study, we designed novel BpT analogues bearing hydrophobic, electron-donating substituents (e.g., methyl, methoxy, or *t*-butyl group) at the *para* position of the noncoordinating phenyl group (RBpT, Figure 1B). This was performed in order to investigate the effects of electron-donating substitutents, and consequently, their lower $Fe^{III/II}$ redox couples, on antiproliferative activity, selectivity, and their ability to catalyze metHb formation. These RBpT ligands exhibited potent and selective antiproliferative activity, which were generally comparable or exceeded that of their parent BpT counterparts. Major findings include that the ability of the *t*-BuBpT series to mediate metHb formation was significantly ($p < 0.05–0.001$) decreased in comparison to 3-AP and Dp44mT in intact red blood cells (RBCs). In fact, levels of oxyHb oxidation mediated by the *t*-BuBpT series, except *t*-BuBpT itself, were comparable to the untreated control. Significantly, examination of their structure–activity relationships suggested that lipophilicity played a role in their limited ability to mediate metHb formation in intact RBCs.

RESULTS AND DISCUSSION

Synthesis and Spectroscopy. The RBpT analogues were all prepared by high yielding Schiff base condensation reactions following previous protocols for related thiosemicarbazones reported from our laboratory.[28,40] The compounds were only sparingly soluble in water. However, they exhibited greater solubility in polar aprotic solvents such as DMF, MeCN, and DMSO. The ^{1}H NMR spectral properties of the RBpT ligands are very similar to those of the BpT analogues.[40] The Fe^{III} complexes were prepared according to previously published procedures.[28,40] They too show limited solubility in water but were soluble in polar organic solvents such as acetone, alcohols (e.g., ethanol), DMF, and DMSO.

Structural Characterization. As a representative example of these analogues, the crystal structure of the free ligand, MeBp44mT, was determined (Table 1 and Supporting

dx.doi.org/10.1021/jm301691s | J. Med. Chem. 2013, 56, 357–370

Table 1. Crystal Data

	MeBp44mT	$[Fe(MeBp44mT)_2]ClO_4$
formula	$C_{16}H_{18}N_4S$	$C_{32}H_{34}ClFeN_8O_4S_2$
formula weight	298.41	750.09
λ (Å)	0.71073	1.54180
crystal system	monoclinic	monoclinic
space group	$P2_1/n$ (no. 14[a])	$P2_1/c$ (no. 14)
color	yellow	black
a (Å)	8.731(3)	11.1769(3)
b (Å)	13.944(7)	16.3295(4)
c (Å)	13.214(5)	19.3586(4)
β (deg)	109.19(4)	90.141(2)
V (Å^3)	1520(1)	3533.2(2)
T (K)	293	293
Z	4	4
R_1 (obsd data)	0.0586	0.0531
wR_2 (all data)	0.1175	0.1521
GOF	1.006	1.027
CCDC no.	899279	899280

[a]Variant of $P2_1/c$.

Information, Figure S1A). The conformation of the ligand finds the pyridyl ring *syn* with respect to the thiosemicarbazide moiety, and hence, the *Z* isomer is present. This isomer is favored by an intramolecular H-bond donated by N3−H to N1. The C13−S1 bond is consistent with a double bond, while the adjacent C13−N3 and C13−N4 bonds are significantly shorter than a single bond, indicating electron delocalization. The observed bond lengths (Supporting Information, Table S1) are similar to other thiosemicarbazones from this family.[28,40]

The crystal structure of the Fe^{III} complex $[Fe(MeBp44mT)_2]ClO_4$ was also determined (Supporting Information, Figure S1B). Both ligands bind as *NNS* chelators in their monoanionic forms. The perchlorate counterion is not shown in Supporting Information Figure S1B. There are no significant differences between the corresponding bond lengths or angles of either ligand (labeled "'*a*" and "'*b*" in Supporting Information Figure S1B and Table S1), and the complex has approximate 2-fold symmetry. Key differences between the structure of the $[Fe(MeBp44mT)_2]^+$ complex and the free ligand, MeBp44mT (Figure S1A) are linked to the deprotonation of N3, which alters the electronic structure of the $NNC(S)NMe_2$ moiety. Most notable is the extension of the C13−S1 bonds in each coordinated ligand from ca. 1.65 to 1.75 Å, effectively now a single bond. That is, the S-donor is effectively a thiolate. This extension of the C13−S1 bond does not significantly alter the adjacent C13−N3 bond, which remains at an intermediate bond length. Interestingly, the more significant variations are to the C13−N4 bonds, which extend slightly upon coordination. This variation in bond length upon coordination is consistent with effective electronic communication of substituent effects on N4. The coordinate bond lengths are again consistent with low spin Fe^{III} and mirror those of other thiosemicarbazone complexes reported in previous studies.[42] The bond angles around the Fe center define a distorted octahedral geometry with the five-membered chelate rings enforcing acute *cis*-coordinate angles (approaching 80°). Hence, as found for other thiosemicarbazones, these agents effectively bind Fe, which is important to note, as their antiproliferative efficacy is directly related to this property.[28,40,42]

Electrochemistry. The electrochemical properties of the Fe complexes of all synthesized ligands were examined by cyclic voltammetry, and the results are summarized in Table 2. Our

Table 2. Partition Coefficients (Log P_{calc}) and $Fe^{III/II}$ Redox Potentials (MeCN:H_2O 7:3) of the RBpT Series Chelators and Their Ferrous and Ferric Complexes[a]

ligand	partition coefficient ($\log P_{calc}$)	$Fe^{III/II}$ redox potential (mV vs NHE)
3-AP		+40[b]
Dp44mT	2.19	+166
BpT	2.25	+113
MeBpT	2.73	+99
MeOBpT	2.12	+91
t-BuBpT	3.95	+98
Bp4mT	2.77	+78
MeBp4mT	3.25	+59
MeOBp4mT	2.64	+52
t-BuBp4mT	4.47	+58
Bp4eT	3.11	+66
MeBp4eT	3.59	+50
MeOBp4eT	2.98	+40
t-BuBp4eT	4.81	+52
Bp44mT	3.14	+62
MeBp44mT	3.63	+47
MeOBp44mT	3.02	+34
t-BuBp44mT	4.85	+49
Bp4pT	4.43	+145
MeBp4pT	4.92	+131
MeOBp4pT	4.31	+126
t-BuBp4pT	6.14	+134

[a]Comparable data for the parent BpT compounds and Dp44mT are also shown. Log P_{calc} values were calculated using the program ChemBioDrawUltra v 11.0.1 using Crippen's fragmentation procedure.[52]. [b]$Fe^{III/II}$ redox potential previously determined in.[36]

previous studies have shown that the biological activity of thiosemicarbazone iron complexes is linked with their capability to undergo Fenton chemistry upon complexation with intracellular iron.[28,40,42−45] All synthesized complexes exhibited totally reversible one electron $Fe^{III/II}$ couples in MeCN:H_2O (7:3) at sweep rates between 50 and 500 mV s^{-1}. This solvent combination was chosen because of the low aqueous solubility of some of the compounds and to enable direct comparison with similar complexes previously prepared by our group.[40] Other solvent combinations such as DMF:H_2O (4:1) also gave similar electrochemistry.

The cathodic shift in the $Fe^{III/II}$ redox potentials of the RBpT complexes in comparison to their corresponding BpT complexes is apparent in Figure 2 and Table 2. As an example, the cyclic voltammograms of four Fe^{III} complexes, namely $[Fe(Bp44mT)_2]^+$, $[Fe(MeBp44mT)_2]^+$, $[Fe(MeOBp44mT)_2]^+$, and $[Fe(t\text{-}BuBp44mT)_2]^+$ bearing the same terminal (N4) substituent ($-NMe_2$) are shown in Figure 2. The redox potentials of the iron RBpT complexes were cathodically shifted by 11−28 mV relative to their parent BpT counterparts (Table 2). This result was anticipated as substituents with electron-donating properties are known to increase the effective negative net charge on neighboring moieties, resulting in a decrease in their redox potentials. The greatest decrease in $Fe^{III/II}$ redox potentials were obtained with the iron complexes derived from the methoxy substituted

dx.doi.org/10.1021/jm301691s | J. Med. Chem. 2013, 56, 357−370

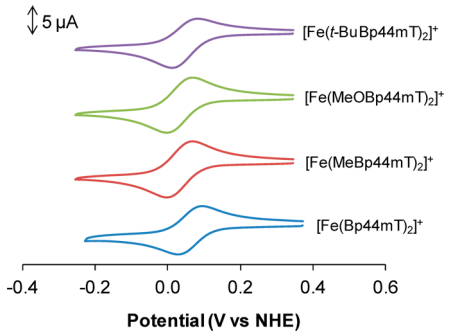

Figure 2. Cyclic voltammograms of ~1 mM solutions of $[Fe(Bp44mT)_2]^+$, $[Fe(MeBp44mT)_2]^+$, $[Fe(MeOBp44mT)_2]^+$, and $[Fe(t\text{-}BuBp44mT)_2]^+$ (from bottom to top), showing the effect of incorporation of various substituents on the $Fe^{III/II}$ redox potential. Sweep rate 100 mV s^{-1}, solvent MeCN:H_2O (70:30) with 0.1 M Et_4NClO_4.

ligands (19−28 mV; Table 2). Substitution with a methyl or *t*-butyl group led to a similar, but smaller cathodic shift of 11−20 mV relative to their corresponding parent BpT iron complexes (Table 2). As expected, for the substitutions examined, resonance effects (i.e., donation of π electrons into the adjacent aromatic ring by the MeO moiety) had a greater impact on the $Fe^{III/II}$ redox potentials than inductive effects (by the Me or *t*-Bu groups), and this is reflected in the lower redox potentials obtained for the iron complexes of the methoxy analogues.

The effect of the identity of the N4 substituents on the $Fe^{III/II}$ redox potential was similar for each RBpT iron complex. That is, the presence of a methyl, ethyl, or dimethyl group at N4 led to a cathodic shift (39−40, 46−51, and 49−57 mV, respectively) in comparison to the parent RBpT iron complex (Table 2). In contrast, the presence of a phenyl group at N4 led to an anodic shift of 32−36 mV relative to the parent RBpT iron complex (Table 2). These trends can be rationalized by the increasing inductive effects of the N4 substituents (i.e., methyl, ethyl, and dimethyl) and the lower electron-donating properties of the phenyl group.

Overall, the incorporation of the methyl, methoxy, and *t*-butyl substituents to the noncoordinating phenyl group led to a reduction in $Fe^{III/II}$ redox potentials for all examined iron complexes (Table 2). In relation to biological activity, all measured $Fe^{III/II}$ redox potentials lie within the range accessible to both cellular oxidants and reductants. Hence, like their BpT counterparts,[40] the iron complexes of the substituted compounds may be able to redox cycle and generate ROS (examined below).

BIOLOGICAL STUDIES

Anti-Proliferative Activity against Tumor Cells. The ability of the RBpT series to inhibit cellular proliferation was assessed using SK-N-MC neuroepithelioma cells, as the effect of iron chelators on their growth has been well characterized.[24,28,40] These novel ligands were compared to their parent compounds, the BpT series,[40] and a number of relevant positive control chelators (Table 3). These controls include: (1) DFO, which is used for the treatment of iron overload,[46] (2) NIH, a ligand with high iron mobilizing activity and modest

Table 3. IC_{50} (μM) Values of RBpT Series Chelators at Inhibiting the Growth of SK-N-MC Neuroepithelioma Cells and Mortal MRC-5 Fibroblasts As Determined by the MTT Assay (72 h)[a]

	IC_{50} (μM)			
ligand	SK-N-MC	MRC-5	*p* value	therapeutic index
DFO	22.7 ± 1.55			
NIH	2.53 ± 0.18			
Dp44mT	0.007 ± 0.002			
3-AP	0.26 ± 0.06[b]			
BpT	3.80 ± 0.84	>12.5	<0.05	>3
MeBpT	0.146 ± 0.045	>12.5	<0.01	>85
MeOBpT	3.950 ± 0.742	>12.5	<0.05	>3
t-BuBpT	0.014 ± 0.004	0.814 ± 0.109	<0.001	58
Bp4mT	0.020 ± 0.002	2.321 ± 0.208	<0.001	116
MeBp4mT	0.015 ± 0.002	2.115 ± 0.495	<0.001	141
MeOBp4mT	0.022 ± 0.002	2.029 ± 0.240	<0.001	92
t-BuBp4mT	0.015 ± 0.002	2.458 ± 0.399	<0.001	164
Bp4eT	0.014 ± 0.003	1.489 ± 0.385	<0.001	106
MeBp4eT	0.013 ± 0.002	2.142 ± 0.807	<0.001	164
MeOBp4eT	0.016 ± 0.002	1.646 ± 0.744	<0.001	102
t-BuBp4eT	0.020 ± 0.003	2.941 ± 0.605	<0.001	147
Bp44mT	0.005 ± 0.001	1.012 ± 0.106	<0.001	202
MeBp44mT	0.007 ± 0.002	0.921 ± 0.137	<0.001	131
MeOBp44mT	0.017 ± 0.005	1.136 ± 0.396	<0.001	66
t-BuBp44mT	0.072 ± 0.006	1.066 ± 0.260	<0.005	15
Bp4pT	0.016 ± 0.004	0.571 ± 0.093	<0.001	36
MeBp4pT	0.024 ± 0.006	1.520 ± 0.610	<0.001	63
MeOBp4pT	0.019 ± 0.002	0.864 ± 0.787	<0.001	45
t-BuBp4pT	0.109 ± 0.028	1.889 ± 0.171	<0.005	17

[a]Results are mean ± SD (three experiments). The *p* values were determined using Student's *t*-test and compare the activity of the ligand in normal and neoplastic cells. Therapeutic index values represent the ratio of MRC-5 to SK-N-MC IC_{50} values, a higher therapeutic index value indicating greater selectivity for neoplastic cells. [b]IC_{50} value previously determined in.[40]

dx.doi.org/10.1021/jm301691s | J. Med. Chem. 2013, 56, 357−370

antiproliferative effects,[24] (3) Dp44mT, a chelator with high antiproliferative activity extensively studied for cancer therapy,[28,29,37] and (4) 3-AP, a thiosemicarbazone under investigation in clinical trials (Figure 1A).[30−32]

This study identified that all of the N4 substituted RBpT analogues (i.e., RBp4mT, RBp4eT, RBp44mT, and RBp4pT), except *t*-BuBp4pT, had high antiproliferative activity against SK-N-MC cells (IC_{50}: 0.007−0.072 μM; Table 3). Interestingly, the most potent analogue, MeBp44mT (IC_{50}: 0.007 ± 0.002 μM), demonstrated similar antiproliferative activity to that of Dp44mT (IC_{50}: 0.007 ± 0.002 μM). The antiproliferative activity of all of the RBpT ligands examined were significantly ($p < 0.001$) more active than DFO (IC_{50}: 22.7 ± 1.55 μM) and, excluding MeOBpT, were all significantly ($p < 0.01$) more active than NIH (IC_{50}: 2.53 ± 0.18 μM). Importantly, excluding MeOBpT, all the RBpT ligands showed 2- to 37-fold greater antiproliferative activity than 3-AP.[40]

The addition of a methyl or *t*-butyl group to the parent BpT ligand for most of these analogues led to the most marked and significant ($p < 0.01$) increase in antiproliferative activity against SK-N-MC neuroepithelioma cells. For these ligands, relative to BpT (IC_{50}: 3.80 ± 0.84 μM), the IC_{50} decreased by 26- and 271-fold for MeBpT (IC_{50}: 0.146 ± 0.045 μM) and *t*-BuBpT (IC_{50}: 0.014 ± 0.004 μM), respectively (Table 3). This marked enhancement in efficacy is thought to be due to the effect of the substituents increasing the lipophilicity of the ligands (Table 2). In contrast, the addition of the methoxy substituent to BpT had no marked effect on the antiproliferative activity, probably because of the similar log P_{calc} value to the parent BpT compound (Table 2).

Because the Bp4mT, Bp4eT, Bp44mT, and Bp4pT compounds are already relatively lipophilic compared to BpT, the addition of lipophilic substituents to these scaffolds, namely methyl, methoxy, and *t*-butyl generally resulted in comparable or only slightly increased antiproliferative activity (Table 3). However, the exception to this observation was that the addition of a *t*-butyl group to Bp44mT and Bp4pT led to a reduction in antiproliferative efficacy, which was significant ($p < 0.01$) for *t*-BuBp4pT relative to the parent compound.

Previously, we demonstrated that the lipophilicity of an iron chelator plays a significant role in their ability to permeate biological membranes, and thus, it is an important factor influencing their biological activity.[24] In the current study, an optimal lipophilic range of the RBpT series was observed to exist, with the most potent antiproliferative ligands possessing log P_{calc} values between 2.5 and 5.0 in SK-N-MC cells, with an optimal efficacy being observed at a log P_{calc} of ∼4 (data not shown). Considering this finding, it is likely that compounds of this class with log P_{calc} values outside this range will either have difficulty traversing the cell membrane by being too hydrophilic or become trapped within membranes due to their high lipophilicity.

Importantly, the incorporation of hydrophobic electron-donating groups in the RBpT series resulted in their iron complexes having lower $Fe^{III/II}$ redox potentials that fall in a range accessible to both cellular oxidants and reductants (e.g., ascorbate, examined below). In fact, the Fe-RBpT complexes are able to undergo facile interconversion between the Fe^{II} and Fe^{III} states. Thus, the ability of the RBpT ligands to gain intracellular access to form an iron complex that generates cytotoxic ROS probably plays a critical role in their antiproliferative effects (Table 3).

Antiproliferative Activity Against Normal Cells. The selectivity of the RBpT series toward neoplastic cells was assessed by examining the antiproliferative activity of the chelators against SK-N-MC neuroepithelioma cells versus mortal MRC-5 fibroblasts is shown in Table 3, and their selectivity was assessed by calculating an in vitro therapeutic index. This parameter represents the ratio of the IC_{50} values of normal to neoplastic cells (i.e., IC_{50} (MRC-5)/IC_{50} (SK-N-MC); Table 3), with higher values representing greater selectivity against tumor cells.

Neoplastic cells were found to be significantly ($p < 0.05$) more sensitive than normal cells to treatment with the chelators, suggesting an appreciable therapeutic index (Table 3). The methyl and *t*-butyl analogues of Bp4mT and Bp4eT displayed the greatest selectivity of the RBpT series ligands, with therapeutic indices of 141 (MeBp4mT), 147 (*t*-BuBp4eT), and 164 (MeBp4eT and *t*-BuBp4mT). However, this therapeutic index was slightly lower than that observed for Bp44mT (202; Table 3). Importantly, the most potent RBpT analogue in terms of antiproliferative activity against SK-N-MC tumor cells, namely MeBp44mT, demonstrated high selectivity, with a therapeutic index of 131 (Table 3).

In agreement with the results found for SK-N-MC tumor cells, an optimal lipophilic range was also observed for MRC-5 cells, with the most potent antiproliferative ligands possessing log P_{calc} values between 2.5 and 5.0 (data not shown). Again, the optimal antiproliferative activity was found at a log P_{calc} of ∼4 and mirrored that identified for SK-N-MC cells. Considering this, there was no marked differential in the optimal log P_{calc} range between mortal MRC5 cells and SK-N-MC tumor cells.

Chelator-Mediated ^{59}Fe Efflux from Cells. As the ability of chelators to bind cellular iron pools plays a role in their antitumor activity,[24] the ability of the RBpT ligands to mobilize intracellular ^{59}Fe from prelabeled SK-N-MC neuroepithelioma cells was examined (Figure 3A). The release of ^{59}Fe mediated by these ligands was compared to that of their parent BpT counterparts as well as the positive controls, DFO, 3-AP, and Dp44mT (Figure 1A), which have been characterized in detail in this cell-type.[11,24,28,40,45,47] As shown previously,[28,40] the control medium alone mediated the release of 5 ± 1% of intracellular ^{59}Fe (Figure 3A), while Dp44mT showed marked ^{59}Fe mobilization efficacy, releasing 38 ± 3% of intracellular ^{59}Fe (Figure 3A). In contrast, the chelators, DFO and 3-AP, demonstrated limited to moderate activity at mobilizing ^{59}Fe, resulting in the release of 12 ± 2% and 25 ± 1% of intracellular ^{59}Fe, respectively.[11,24,28,40]

All methyl and methoxy analogues of BpT, Bp4mT, Bp4eT, and Bp44mT demonstrated high ^{59}Fe mobilization activity, resulting in the release of 32−38% of cellular ^{59}Fe (Figure 3A). These methyl- and methoxy-substituted compounds were comparable to both the parent BpT ligands and Dp44mT, but were significantly ($p < 0.01$) more effective than DFO at releasing cellular ^{59}Fe. Interestingly, the *t*-butyl analogues were significantly ($p < 0.01$) less effective at releasing cellular ^{59}Fe than their parent BpT analogues. Substitution of Bp4pT with either the methyl, methoxy, or *t*-butyl moiety led to a significant ($p < 0.01$) reduction in ^{59}Fe mobilization activity, resulting in activity comparable to that of DFO. This latter group represents the most lipophilic ligands (Table 2) and, as such, may become entrapped within membranes or other lipophilic compartments in cells and this may explain their inability to

dx.doi.org/10.1021/jm301691s | J. Med. Chem. 2013, 56, 357−370

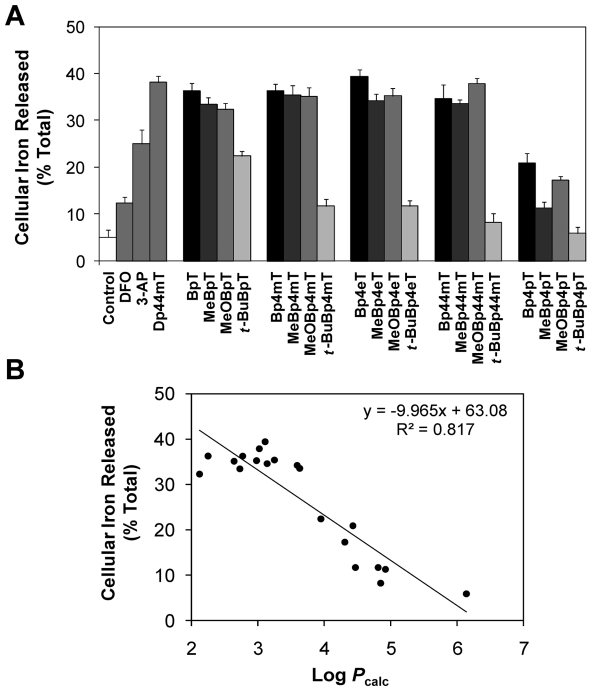

Figure 3. (A) The effect of the RBpT series chelators (25 μM) on ^{59}Fe mobilization from prelabeled SK-N-MC neuroepithelioma cells. Results are mean ± SD of three experiments with three determinations in each experiment. (B) The relationship between ^{59}Fe mobilization and lipophilicity (log P_{calc}) of the RBpT analogues.

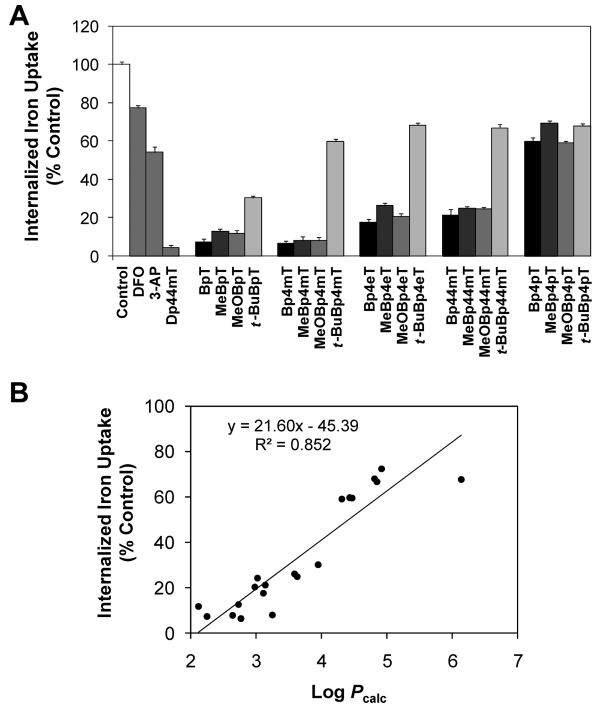

Figure 4. (A) The effect of the RBpT series chelators (25 μM) on internalized ^{59}Fe uptake from ^{59}Fe-transferrin (^{59}Fe-Tf) by SK-N-MC neuroepithelioma cells. Results are mean ± SD of three experiments with three determinations in each experiment. (B) The relationship between ^{59}Fe uptake and lipophilicity (log P_{calc}) of the RBpT ligands.

induce ^{59}Fe efflux. However, no relationship (R^2 = 0.32) between the IC_{50} values and iron mobilization was demonstrated, indicating other factors are also important in terms of their antiproliferative activity.

Importantly, plotting ^{59}Fe mobilization against lipophilicity (log P_{calc}) yielded a linear relationship (R^2 = 0.817; Figure 3B), demonstrating that increased lipophilicity decreased iron mobilization efficacy. Collectively, these results illustrate the important role optimum lipophilicity plays in binding and mobilizing iron from cellular iron pools.[10,46,48]

Chelator-Mediated Inhibition of Cellular ^{59}Fe Uptake from ^{59}Fe-Transferrin. The ability of the RBpT series chelators to inhibit ^{59}Fe uptake from the iron transport protein, Tf, by SK-N-MC neuroepithelioma cells, was also assessed (Figure 4A). This was examined as inhibiting cancer cell proliferation through iron deprivation involves both iron mobilization and preventing iron uptake from Tf.[24] As demonstrated in our previous work,[28,40] the positive control, Dp44mT, was found to effectively reduce ^{59}Fe uptake to 4 ± 1% of the control (Figure 4A). In contrast, the ligands, DFO and 3-AP, exhibited far less activity, as previously shown,[11,24,28,40] reducing ^{59}Fe uptake to only 77 ± 1% and 54 ± 3% of the control, respectively (Figure 4A).

All methyl and methoxy analogues of BpT, Bp4mT, Bp4eT, and Bp44mT markedly reduced ^{59}Fe uptake to 8−26% of the control value (Figure 4A), being significantly (p < 0.01) more effective than DFO. However, all substituted ligands examined were significantly (p < 0.01) less effective than Dp44mT at inhibiting ^{59}Fe uptake from ^{59}Fe-Tf. The methyl and methoxy analogues of BpT and Bp4mT were the most effective RBpT ligands at reducing ^{59}Fe uptake from ^{59}Fe-Tf, decreasing it to 8 − 13% of the control (Figure 4A). As observed in ^{59}Fe efflux experiments (Figure 3A), the *t*-butyl analogues were significantly (p < 0.01) less effective at inhibiting ^{59}Fe uptake from ^{59}Fe-Tf than their parent analogues. All Bp4pT analogues were found to possess the lowest activity at inhibiting ^{59}Fe uptake. However, despite their low activity, they were all significantly (p < 0.01) more effective at inhibiting ^{59}Fe uptake than DFO. Notably, there was little correlation (R^2 = 0.31) between the IC_{50} values and the inhibition of iron uptake (data not shown), demonstrating that other factors apart from Fe deprivation play a role in the antiproliferative activity.

As found for iron mobilization studies, a correlation between lipophilicity and inhibition of iron uptake was observed, yielding a linear relationship (R^2 = 0.852; Figure 4B). These results indicate an important role for optimum lipophilicity in inhibiting iron uptake from Tf.

Ascorbate Oxidation Studies. The cyclic voltammetry experiments reported above (Table 2) suggest that the iron complexes of the RBpT ligands can undergo facile interconversion between the ferric and ferrous states. This occurred at potentials accessible to both biological reductants and oxidants, indicating that the iron complexes of these novel ligands may participate in the generation of ROS[49] and result in their enhanced antiproliferative activity. Hence, it was important to confirm the ability of the RBpT iron complexes to mediate the oxidation of a physiological substrate. Thus, the oxidation of ascorbate catalyzed by the iron complexes of the RBpT analogues was assessed in comparison to their parent BpT counterparts (Figure 5). Both EDTA and Dp44mT were also included to act as positive controls, as the ability of their iron complexes to mediate ascorbate oxidation has been well characterized.[28,40,42,47]

In these studies, the results are expressed as iron-binding equivalents (IBE) due to the different denticity of the chelators

dx.doi.org/10.1021/jm301691s | J. Med. Chem. 2013, 56, 357−370

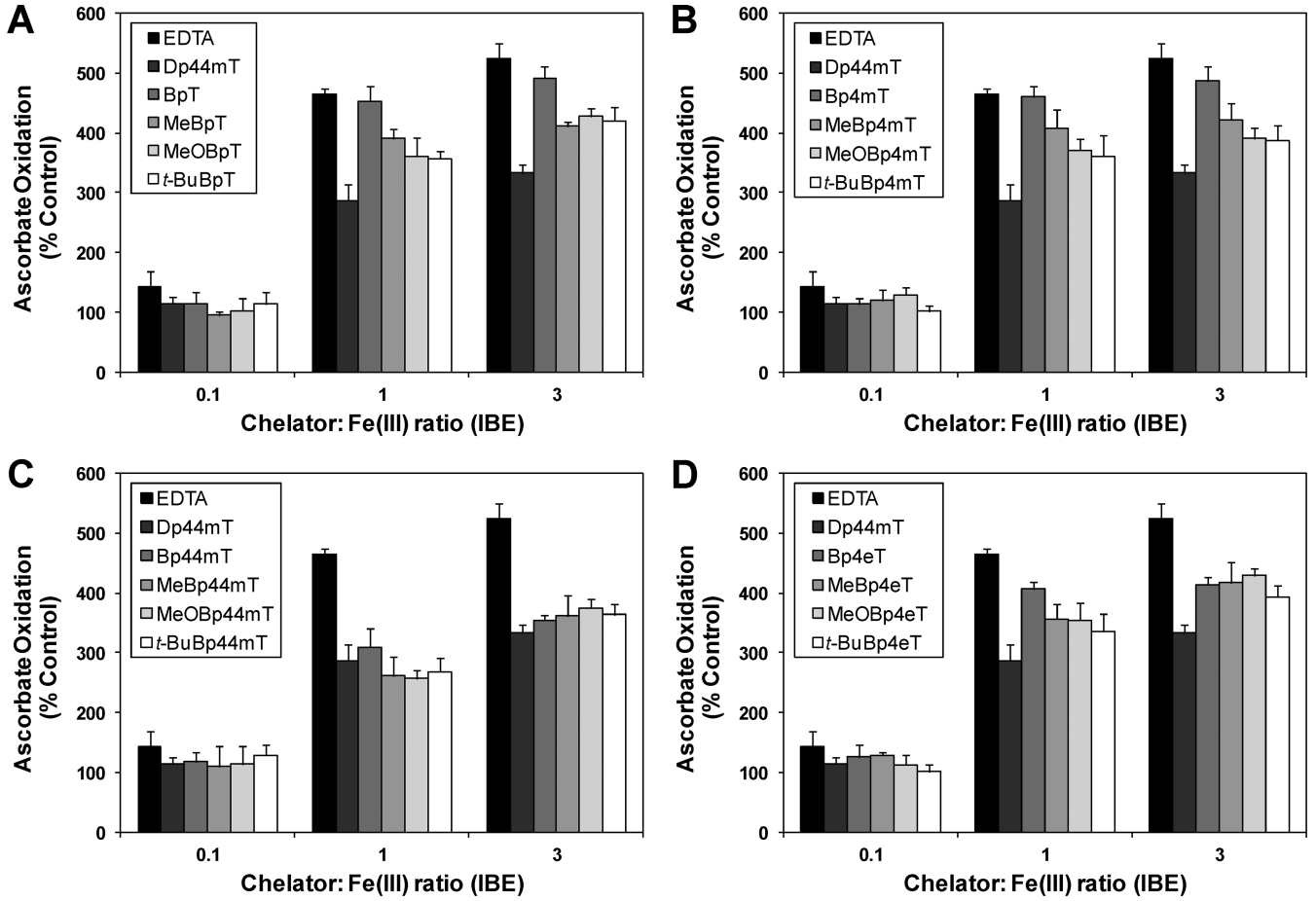

Figure 5. The effect of the Fe^{III} complexes of the: (A) RBpT, (B) RBp4mT, (C) RBp44mT, and (D) RBp4eT series relative to their parent BpT compounds on ascorbate oxidation. Comparison of these chelators is made to the positive controls, EDTA, and Dp44mT. Results are mean ± SD (three experiments).

examined (i.e., EDTA is hexadentate and forms 1:1 iron/ligand complexes, while the RBpT and BpT series and Dp44mT are tridentate chelators and form 1:2 iron/ligand complexes). A range of IBE ratios were examined, namely 0.1, 1, and 3. An IBE of 0.1 corresponds to an excess of iron to chelator (i.e., 1 hexadentate or 2 tridentate chelators in the presence of 10 atoms of iron), while an IBE of 1 represents a completely filled coordination sphere (i.e., the formation of a 1:1 EDTA iron complex or a 2:1 tridentate thiosemicarbazone iron complex). On the other hand, an IBE of 3 is equivalent to an excess of chelator to iron, representing 3 hexadentate or 6 tridentate ligands for each iron atom.[28,40,42,47] These studies were performed in buffer containing acetonitrile (25% v/v) to ensure the solubility of the ligands during the assay. However, the ligands containing the phenyl group at the terminal N4 position (i.e., RBp4pT) were not able to be dissolved due to their highly hydrophobic nature and thus were not able to be assessed.

At all IBEs assessed, the iron EDTA complex demonstrated the greatest activity at increasing ascorbate oxidation (Figure 5). For all iron chelator complexes, a marked increase in ascorbate oxidation was found upon increasing the IBE from 0.1 to 1 and 3. All iron complexes of the RBpT analogues showed similar activity to their parent ligands at oxidizing ascorbate. In fact, apart from Bp44mT and the RBp44mT analogues, the rest of the RBpT analogues and their parent compounds were significantly ($p < 0.05$) more effective than Dp44mT at oxidizing ascorbate (Figure 5). We have previously demonstrated that the iron Dp44mT complex is more effective than iron-3-AP at mediating ascorbate oxidation.[28] Hence, as found for similar thiosemicarbazones,[28,40,42,47] the iron complexes of the new RBpT analogues show considerable redox activity.

Methemoglobin Formation. A considerable therapeutic index is a desirable factor in the design of novel anticancer agents that specifically target cancer cells with minimal side effects. Importantly, methemoglobinemia and hypoxia are notable side effects associated with the clinical administration of the chelator, 3-AP.[33−35] These detrimental effects are critical to consider in the design of novel iron chelators as anticancer agents.

We previously demonstrated that the ability of 3-AP to form a redox active iron complex is an important factor in the formation of metHb, an oxidation product of oxyHb that cannot bind oxygen.[36] Considering that the iron complexes of our novel RBpT analogues are also redox active (Figures 2 and 5), it was vital to assess their ability to mediate metHb formation as this may provide an insight into their tolerability in vivo. In these studies, the RBpT series of ligands and their iron complexes (25 μM) were incubated with RBC lysates or intact RBCs for 3 h/37 °C and metHb formation was assessed by standard methods.[36,50] This was carried out in comparison to the positive control chelators, Dp44mT and 3-AP, and their

dx.doi.org/10.1021/jm301691s | J. Med. Chem. 2013, 56, 357−370

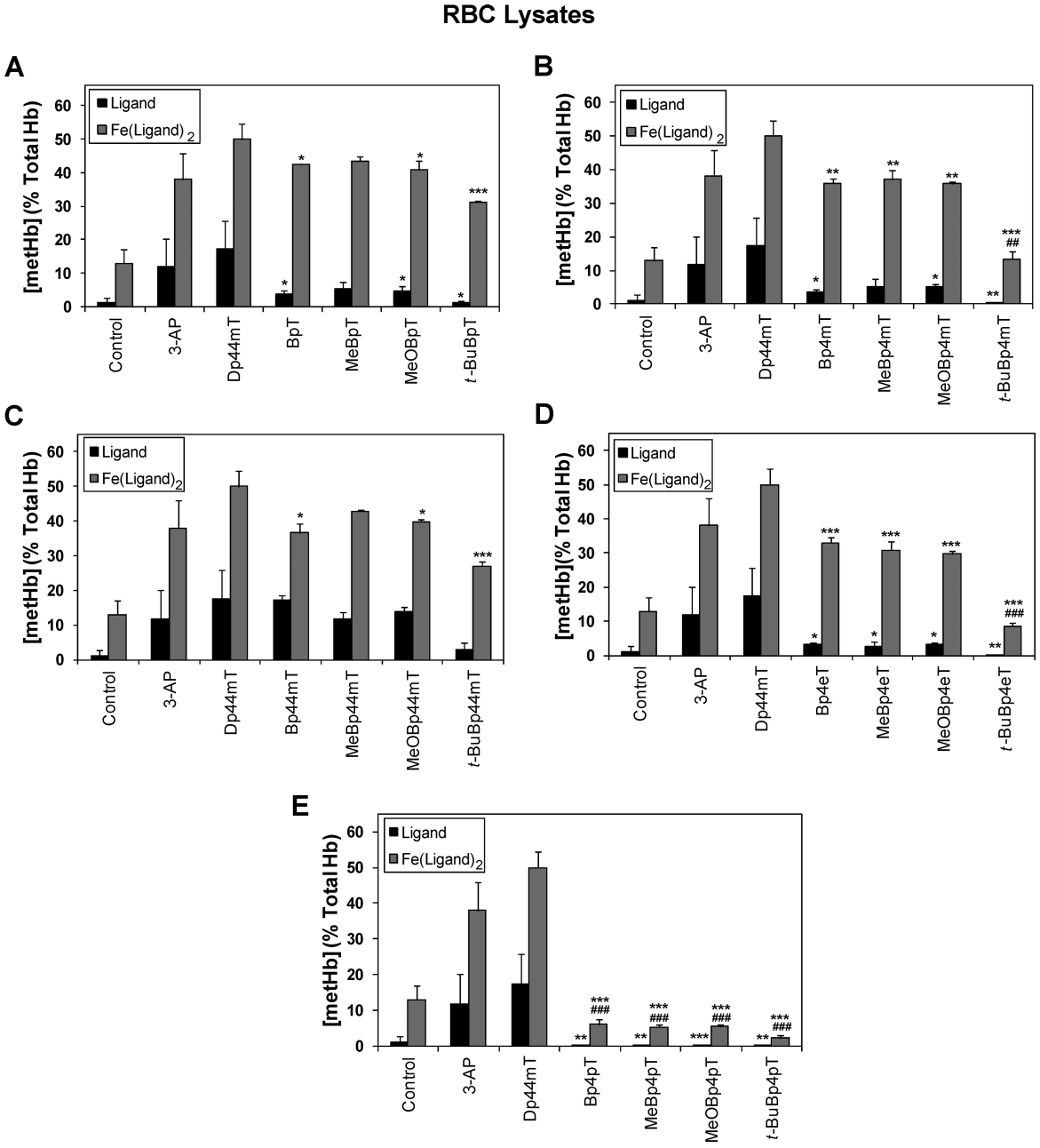

Figure 6. MetHb formation in RBC lysates by the thiosemicarbazones, 3-AP and Dp44mT, after a 3 h incubation at 37 °C in comparison to: (A) BpT, MeBpT, MeOBpT and *t*-BuBpT, (B) Bp4mT, MeBp4mT, MeOBp4mT, and *t*-BuBp4mT, (C) Bp44mT, MeBp44mT, MeOBp44mT, and *t*-BuBp44mT, (D) Bp4eT, MeBp4eT, MeOBp4eT, and *t*-BuBp4eT, (E) Bp4pT, MeBp4pT, MeOBp4pT, and *t*-BuBp4pT and their corresponding iron complexes (25 μM). Results are mean ± SD (3 experiments). *$p < 0.05$, **$p < 0.01$, ***$p < 0.001$, * ligand or iron complex vs Dp44mT or the Dp44mT iron complex, respectively. $^{\#\#}p < 0.01$, $^{\#\#\#}p < 0.001$, $^{\#}$ iron complex vs the 3-AP iron complex.

iron complexes, as their ability to catalyze the formation of metHb has been previously characterized.[36]

In RBC lysates, Dp44mT and 3-AP were able to significantly ($p < 0.01–0.05$) increase oxyHb oxidation, leading to 12 ± 8% and 17 ± 8% metHb generation, respectively, relative to the control (1.2 ± 1.5%; Figure 6), as previously described.[36] As expected, their iron complexes ($Fe(Ligand)_2$) were significantly ($p < 0.001$) more effective at oxidizing oxyHb than the free ligand alone in RBC lysates (Figure 6), demonstrating the formation of a redox active iron complex is essential to mediate metHb generation.[36] All BpT and RBpT ligands, except MeBpT, MeBp4mT, and those containing the dimethyl substituent at the N4 terminal atom, mediated significantly ($p < 0.05–0.001$) decreased levels of metHb generation than Dp44mT. Moreover, all BpT and RBpT iron complexes, except those of MeBpT and MeBp44mT, displayed significantly ($p < 0.05–0.001$) reduced levels of oxyHb oxidation than the Dp44mT iron complex (Figure 6). Additionally, the iron complexes of all BpT and RBpT ligands having the phenyl substituent at the N4 position (Figure 6E) and also *t*-BuBp4mT and *t*-BuBp4eT showed significantly ($p < 0.01–0.001$) decreased metHb levels in comparison to the iron complex of 3-AP. Interestingly, the ability of RBpT ligands containing either an ethyl (Figure 6D) or phenyl (Figure 6E) substitutent at the N4 position to mediate metHb formation was the lowest of the ligands examined in RBC lysates, with the free ligands

dx.doi.org/10.1021/jm301691s | J. Med. Chem. 2013, 56, 357–370

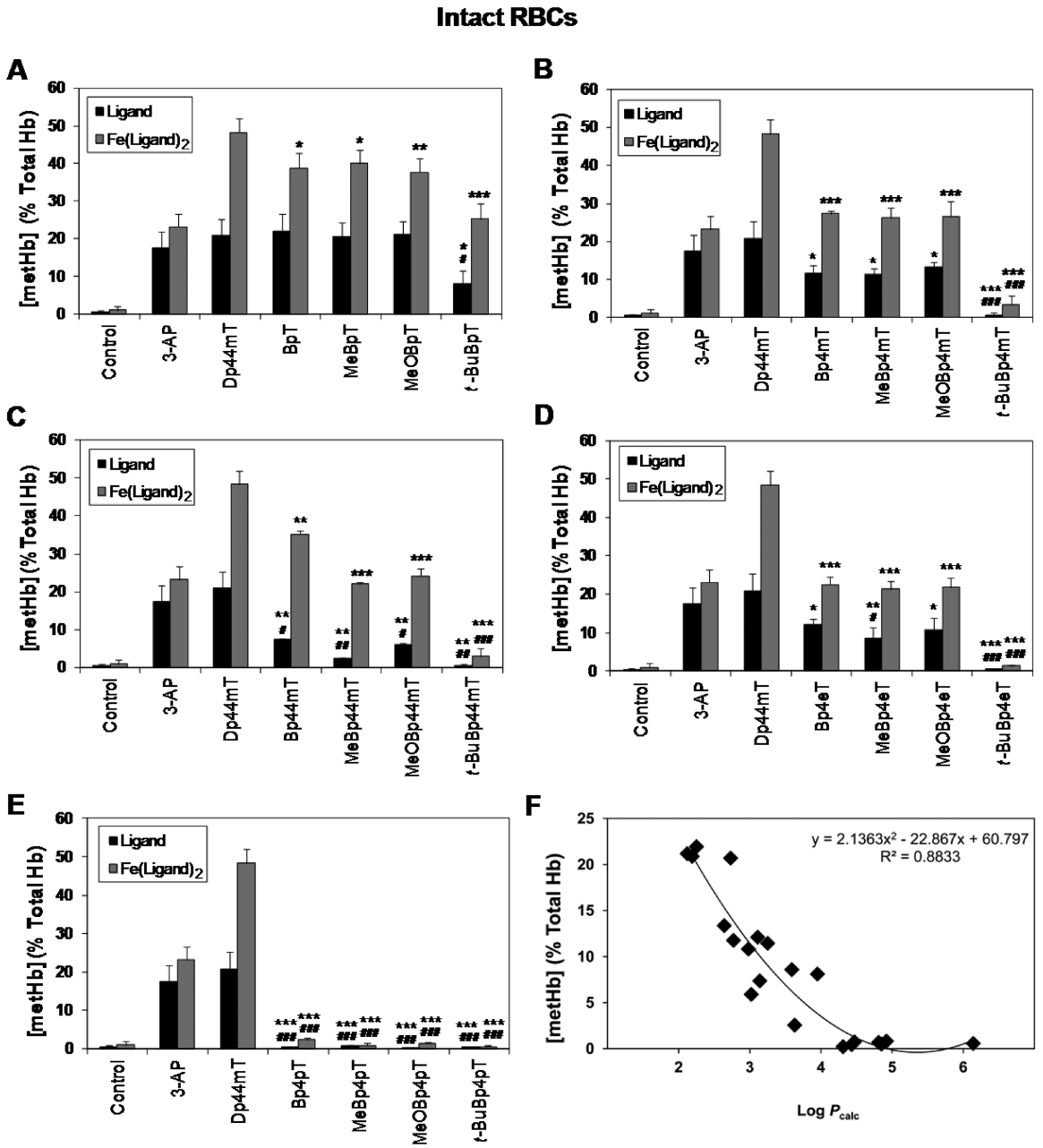

Figure 7. MetHb formation in intact RBCs after a 3 h incubation at 37 °C with the thiosemicarbazones, 3-AP and Dp44mT, in comparison to: (A) BpT, MeBpT, MeOBpT, and *t*-BuBpT, (B) Bp4mT, MeBp4mT, MeOBp4mT, and *t*-BuBp4mT, (C) Bp44mT, MeBp44mT, MeOBp44mT, and *t*-BuBp44mT, (D) Bp4eT, MeBp4eT, MeOBp4eT, and *t*-BuBp4eT, (E) Bp4pT, MeBp4pT, MeOBp4pT, and *t*-BuBp4pT and their corresponding iron complexes (25 μM). Results are mean ± SD (three experiments). (F) The relationship between metHb generation and lipophilicity (log P_{calc}) of the BpT and RBpT ligands. *$p < 0.05$, **$p < 0.01$, ***$p < 0.001$, * ligand or iron complex vs Dp44mT or the Dp44mT iron complex, respectively. $^{\#}p < 0.05$, $^{\#\#}p < 0.01$, $^{\#\#\#}p < 0.001$, # ligand or iron complex vs 3-AP or the 3-AP iron complex, respectively.

being comparable to that of the control. Analysis of their structure−activity relationships regarding metHb generation as a function of their lipophilicity or $Fe^{III/II}$ redox potentials did not demonstrate any relationship, suggesting that other factors are important in this reaction in RBCs lysates.

In intact RBCs, the ligands, 3-AP and Dp44mT, were similarly able to catalyze the oxidation of oxyHb to metHb, resulting in a significant ($p < 0.001$) 38- and 45-fold increase in metHb levels, respectively, relative to the control (Figure 7). As previously observed,[36] the iron complex of Dp44mT was significantly ($p < 0.001$) more effective at oxidizing oxyHb than the free ligand alone, demonstrating that the formation of the iron complex was crucial in this mechanism. In fact, the iron complex of Dp44mT mediated a 2.3-fold increase in oxyHb oxidation in comparison to the free ligand in intact RBCs (Figure 7). In general, all the BpT chelators and their corresponding RBpT analogues, except the more hydrophilic parent compounds, BpT, MeBpT, and MeOBpT, mediated significantly ($p < 0.05$−0.001) lower levels of oxyHb oxidation than Dp44mT (Figure 7). The levels of metHb catalyzed by the iron complexes of the BpT and RBpT ligands were significantly ($p < 0.05$−0.001) decreased relative to that of the iron complex of Dp44mT in intact RBCs (Figure 7). Additionally, the more lipophilic BpT and RBpT ligands containing either a dimethyl

dx.doi.org/10.1021/jm301691s | J. Med. Chem. 2013, 56, 357−370

(Figure 7C) or phenyl (Figure 7E) substituent at the N4 terminal atom, as well as MeBp4eT and all chelators of the hydrophobic *t*-BuBpT series, demonstrated significantly ($p < 0.05–0.001$) decreased oxyHb oxidation than 3-AP. Similarly, iron complexes of the BpT and RBpT ligands containing a terminal N4 phenyl substituent (Figure 7E) and all iron complexes of the *t*-BuBpT series, except the relatively hydrophilic parent *t*-BuBpT ligand, mediated significantly ($p < 0.001$) decreased levels of metHb than the iron complex of 3-AP. Importantly, the levels of oxyHb oxidation observed in intact RBCs in the presence of the *t*-BuBpT ligands, except *t*-BuBpT itself, and the BpT and RBpT chelators containing a terminal N4 phenyl substituent were the lowest of all the ligands examined, being comparable to that of the control (Figure 7).

Collectively, these studies in the more physiologically relevant intact RBC system demonstrated that the ability of RBpT ligands to catalyze metHb formation correlated with lipophilicity ($R^2 = 0.8833$; Figure 7F). In fact, the more lipophilic ligands (e.g., *t*-BuBp4mT, *t*-BuBp44mT, *t*-BuBp4eT, and *t*-BuBp4pT) did not induce marked oxyHb oxidation, with levels being comparable to the untreated control. These observations indicate that lipophilic chelators and/or their iron complexes may be sequestered in hydrophobic environments, reducing their availability to interact with and oxidize oxyHb.

CONCLUSIONS

The development of novel chemotherapeutics that have a high therapeutic index are required to selectively target cancer without inducing deleterious side effects. Previously, methemoglobinemia and hypoxia were noted as side effects associated with the clinical administration of the iron chelator, 3-AP.[33−35] These detrimental effects are a major concern in patients with compromised cardiopulmonary function and are critical to consider in the future design of novel iron chelators as anticancer agents. In the current investigation, we examined the effect of a reduction in $Fe^{III/II}$ redox potentials, achieved by incorporating hydrophobic, electron-donating substitutents at the *para* position of the noncoordinating phenyl group (RBpT series) on antiproliferative activity and metHb generation.

The addition of an electron-donating group led to a group-dependent reduction in the redox potential of RBpT-Fe complexes in comparison to that of their parent BpT iron complexes. However, all measured $Fe^{III/II}$ redox potentials were found to lie within the range accessible to both cellular oxidants and reductants, suggesting their ability to redox cycle in biological systems. This was supported by the ability of the RBpT iron complexes to catalyze the oxidation of ascorbate and suggests that their ability to redox cycle may play a role in their antiproliferative effects. Indeed, these RBpT ligands exhibited potent and selective antiproliferative activity, being generally comparable or exceeding that of their BpT counterparts.

A major finding of these studies was that the levels of metHb formation mediated by the *t*-BuBpT series was significantly ($p < 0.05–0.001$) reduced in comparison to that catalyzed by 3-AP and Dp44mT in intact RBCs. In fact, levels of oxyHb oxidation mediated by the *t*-BuBpT series, except the *t*-BuBpT ligand itself, were comparable to the control and demonstrate the lowest levels of metHb generation of any thiosemicarbazone examined by our group to date. These studies suggested that the ability of the ligand to gain intracellular access to oxidize oxyHb via its iron complex was dependent on their lipophilicity, and this was a key determinant in the formation of metHb in intact RBCs. This observation was further supported by the limited ability of the lipophilic *t*-BuBpT ligands to effectively mobilize intracellular ^{59}Fe, suggesting that they may be sequestered in hydrophobic intracellular compartments. Collectively, these data indicate the RBpT analogues exhibit potent anticancer activity in vitro without displaying the adverse effects (e.g., metHb generation) associated with 3-AP administration.

EXPERIMENTAL PROCEDURES

All commercial reagents were used without further purification. Desferrioxamine (DFO) was obtained from Novartis (Basel, Switzerland). The 2′-(4″-methoxybenzoyl)pyridine, 2′-(4″-methylbenzoyl)-pyridine, and 2′-(4″-*t*-butylbenzoyl)pyridine precursors were obtained from Rieke Metals Inc. (Lincoln, USA). The chelator, Dp44mT was prepared and characterized according to previously described methods.[28] 3-AP was synthesized by standard methods.[51] Combustion analysis (C, H, N) of the ligands and complexes was performed to demonstrate ≥95% purity.

Physical Methods. ^1H NMR (400 MHz) spectra were acquired using a Bruker Avance 400 NMR spectrometer with DMSO-d_6 as the solvent and internal reference (Me_2SO: ^1H NMR δ 2.49 ppm and ^{13}C NMR δ 39.5 ppm vs TMS). Infrared spectra were measured with a Varian Scimitar 800 FT-IR spectrophotometer, with compounds being dispersed as KBr discs. Cyclic voltammetry was performed using a BAS100B/W potentiostat. A glassy carbon working electrode, an aqueous Ag/AgCl reference and Pt wire auxiliary electrode were used. All complexes were at ca. 1 mM concentration in MeCN:H_2O 70:30 v/v. This solvent combination was used to ensure solubility of all complexes. The supporting electrolyte was Et_4NClO_4 (0.1 M), and the solutions were purged with nitrogen prior to measurement. All potentials are cited vs the NHE by addition of 196 mV to the potentials measured relative to the Ag/AgCl reference electrode. Calculated partition coefficients of the free ligands were determined by ChemBioDraw v.11.0.1. (CambridgeSoft) using Crippen's fragmentation procedure.[52]

Crystallography. Intensity data were acquired on an Oxford Diffraction Gemini Ultra S CCD diffractometer. Data reduction was performed with the CrysAlisPro program (version 171.33.42). The structures were solved by direct methods with SHELX-86 and refined by full matrix least-squares with SHELXL.[53] Thermal ellipsoid diagrams were generated with ORTEP3.[54] All calculations were carried out within the WinGX package.[55]

Chelators of the RBpT Series: General Synthesis. The ligands were synthesized by the following general procedure: 2′-(4″-alkylbenzoyl)pyridine (0.01 mol) was dissolved in ethanol (5 mL) and subsequently the appropriate thiosemicarbazide (1.00 g, 0.01 mol) was dissolved in ethanol (5 mL) and the two solutions then mixed. Glacial acetic acid (5−6 drops) was added and the mixture gently refluxed for 2−5 h. The mixture was cooled to room temperature and allowed to stand in a refrigerator overnight to ensure complete precipitation. The product was filtered off and washed with ethanol (10 mL), followed by diethyl ether (10 mL).

p-Methyl-2-benzoylpyridine Thiosemicarbazone (MeBpT). Pale-yellow powder (yield: 74%). Anal. Calcd for $C_{14}H_{14}N_4S·1/4H_2O$: C, 61.18; H, 5.32; N, 20.38%. Found: C, 61.02; H, 5.19; N, 20.39%. ^1H NMR (DMSO-d_6): 12.30 (s, 1H), 8.58 (s, 1H), 8.15 (s, 1H), 8.02 (td, 1H), 7.61 (td, 1H), 8.86 (d, 1H), 7.38 (d, 1H), 7.54 (d, 2H), 7.24 (d, 2H), 2.36 (s, 3H). MS (EI) m/z 270 (M^+). Crystals of this compound suitable for X-ray work were formed from the reaction mixture.

p-Methyl-2-benzoylpyridine 4-methyl-3-thiosemicarbazone (MeBp4mT). Pale-yellow powder (yield: 81%). Anal. Calcd for $C_{15}H_{16}N_4S$: C, 63.35; H, 5.67; N, 19.71%. Found: C, 63.12; H, 5.66; N, 19.70%. ^1H NMR (DMSO-d_6): 12.56 (s, 1H), 8.86 (dq, 1H), 8.69 (q, 1H), 8.01 (td, 1H), 7.60 (td, 1H), 7.36 (dt, 1H), 7.53 (d, 2H), 7.26 (d, 2H), 3.04 (d, 3H), 2.36 (s, 3H). MS (EI) m/z 284 (M^+).

p-Methyl-2-benzoylpyridine 4-ethyl-3-thiosemicarbazone (MeBp4eT). Pale-yellow crystals (yield: 89%). Anal. Calcd for $C_{16}H_{18}N_4S$:

dx.doi.org/10.1021/jm301691s | J. Med. Chem. 2013, 56, 357−370

C, 64.39; H, 6.08; N, 18.78%. Found: C, 64.15; H, 5.99; N, 18.82%. ^{1}H NMR (DMSO-d_6): 12.50 (s, 1H), 8.86 (d, 1H), 8.73 (tr, 1H), 7.36 (d, 1H), 8.01. (td, 1H), 7.60 (td, 1H), 7.53 (d, 2H), 7.26 (d, 2H), 3.61 (q, 2H), 2.37 (s, 3H), 1.15 (tr, 3H). MS (EI) m/z 298 (M^+).

p-Methyl-2-benzoylpyridine 4,4-Dimethyl-3-thiosemicarbazone (MeBp44mT). Yellow crystals (yield: 78%). Anal. Calcd for $C_{16}H_{18}N_4S$: C, 64.39; H, 6.08; N, 18.78%. Found: C, 64.36; H, 6.1; N, 18.99%. ^{1}H NMR (DMSO-d_6): 8.86 (d, 1H), 7.36 (d, 1H), 8.01. (td, 1H), 7.59 (td, 1H), 7.43 (d, 2H), 7.29 (d, 2H), 3.34 (d, 6H), 2.37 (s, 3H). MS (EI) m/z 298 (M^+).

p-Methyl-2-benzoylpyridine 4-Phenyl-3-thiosemicarbazone (MeBp4pT). Yellow crystals (yield: 69%). Anal. Calcd for $C_{20}H_{18}N_4S\cdot 1/2H_2O$: C, 67.58; H, 5.39; N, 15.76%. Found: C, 67.87; H, 5.39; N, 15.8%. ^{1}H NMR (DMSO-d_6): 12.86 (s, 1H), 10.28 (s, 1H), 8.87 (d, 1H), 8.05. (td, 1H), 7.63 (td, 1H), 7.62 (d, 2H), 7.57 (d, 2H), 7.42 (tr, 1H), 7.40 (tr, 2H), 7.37 (d, 1H), 7.27 (d, 2H), 2.37 (s, 3H). MS (EI) m/z 346 (M^+).

p-Methoxy-2-benzoylpyridine Thiosemicarbazone (MeOBpT). Yellow powder (yield: 82%). Anal. Calcd for $C_{14}H_{14}ON_4S$: C, 58.72; H, 4.93; N, 19.57%. Found: C, 58.37; H, 4.90; N, 19.69%. ^{1}H NMR (DMSO-d_6): 12.30 (s, 1H), 8.86 (d, 1H), 8.58 (s, 1H), 8.15 (s, 1H), 8.02 (td, 1H), 7.61 (td, 1H), 7.54 (d, 2H), 7.38 (d, 1H), 7.24 (d, 2H), 2.36 (s, 3H). MS (EI) m/z 286 (M^+).

p-Methoxy-2-benzoylpyridine 4-Methyl-3-thiosemicarbazone (MeOBp4mT). Bright-yellow crystals (yield: 89%). Anal. Calcd for $C_{15}H_{16}ON_4S\cdot 1/4H_2O$: C, 59.09; H, 5.45; N, 18.38%. Found: C, 59.11; H, 5.23; N, 18.48%. ^{1}H NMR (DMSO-d_6): 12.56 (s, 1H), 8.86 (dq, 1H), 8.69 (q, 1H), 8.01 (td, 1H), 7.60 (td, 1H), 7.53 (d, 2H), 7.36 (dt, 1H), 7.26 (d, 2H), 3.04 (d, 3H), 2.36 (s, 3H). MS (EI) m/z 300 (M^+).

p-Methoxy-2-benzoylpyridine 4-Ethyl-3-thiosemicarbazone (MeOBp4eT). Bright-yellow crystals (yield: 80%). Anal. Calcd for $C_{16}H_{18}ON_4S$: C, 61.12; H, 5.77; N, 17.82%. Found: C, 60.95; H, 5.83; N, 17.78%. ^{1}H NMR (DMSO-d_6): 12.50 (s, 1H), 8.86 (d, 1H), 8.73 (tr, 1H), 8.01 (td, 1H), 7.60 (td, 1H), 7.53 (d, 2H), 7.36 (d, 1H), 7.26 (d, 2H), 3.61 (q, 2H), 2.37 (s, 3H), 1.15 (tr, 3H). MS (EI) m/z 314 (M^+).

p-Methoxy-2-benzoylpyridine 4,4-dimethyl-3-thiosemicarbazone (MeOBp44mT). Orange crystals (yield: 81%). Anal. Calcd for $C_{16}H_{18}ON_4S\cdot 1/2H_2O$: C, 59.42; H, 5.92; N, 17.32%. Found: C, 59.86; H, 5.71; N, 16.94%. ^{1}H NMR (DMSO-d_6): 8.86 (d, 1H), 8.01 (td, 1H), 7.59 (td, 1H), 7.43 (d, 2H), 7.36 (d, 1H),7.29 (d, 2H), 3.34 (d, 6H), 2.37 (s, 3H). MS (EI) m/z 314 (M^+).

p-Methoxy-2-benzoylpyridine 4-phenyl-3-thiosemicarbazone (MeOBp4pT). Orange powder (yield: 70%). Anal. Calcd for $C_{20}H_{18}ON_4S$: C, 66.27; H, 5.01; N, 15.46%. Found: C, 67.27; H, 5.16; N, 15.77%. ^{1}H NMR (DMSO-d_6): 12.86 (s, 1H), 10.28 (s, 1H), 8.87 (d, 1H), 8.05 (td, 1H), 7.63 (td, 1H), 7.62 (d, 2H), 7.57 (d, 2H), 7.42 (tr, 1H), 7.40 (tr, 2H), 7.37 (d, 1H), 7.27 (d, 2H), 2.37 (s, 3H). MS (EI) m/z 362 (M^+).

p-t-Butyl-2-benzoylpyridine Thiosemicarbazone (t-BuBpT). Pale-yellow powder (yield: 84%). Anal. Calcd for $C_{17}H_{20}N_4S$: C, 65.43; H, 6.45; N, 17.93%. Found: C, 65.43; H, 6.56; N, 17.95%. ^{1}H NMR (DMSO-d_6): 12.50 (s, 1H), 8.85 (d, 1H), 8.56 (s, 1H), 8.12 (s, 1H), 8.00 (td, 1H), 7.60 (td, 1H), 7.55 (d, 2H), 7.43 (d, 2H), 7.37 (d, 1H), 1.32 (s, 9H). MS (ESI) m/z 313 (MH^+).

p-t-Butyl-2-benzoylpyridine 4-Methyl-3-thiosemicarbazone (t-BuBp4mT). Yellow crystals (yield: 77%). Anal. Calcd for $C_{18}H_{22}N_4S\cdot H_2O$: C, 62.76; H, 7.02; N, 16.26%. Found: C, 62.53; H, 6.57; N, 16.18%. ^{1}H NMR (DMSO-d_6): 12.77 (s, 1H), 8.85 (d, 1H), 8.02 (td, 1H), 7.59 (td, 1H), 7.53 (d, 2H), 7.45 (d, 2H), 7.37 (d, 2H), 3.04 (d, 3H), 1.30 (s, 9H). MS (EI) m/z 326 (M^+).

p-t-Butyl 2-Benzoylpyridine 4-Ethyl-3-thiosemicarbazone (t-BuBp4eT). Bright-yellow crystals (yield: 88%). Anal. Calcd for $C_{19}H_{24}N_4S$: C, 66.82; H, 7.38; N, 16.41%. Found: C, 66.70; H, 7.23; N, 16.27%. ^{1}H NMR (DMSO-d_6): 12.77 (s, 1H), 8.84 (d, 1H), 8.71 (t, 1H), 7.99 (td, 1H), 7.58 (td, 1H), 7.53 (d, 2H), 7.45 (d, 2H), 7.34 (d, 1H), 3.57 (q, 2H), 1.31 (s, 9H), 1.11 (t, 3H). MS (EI) m/z 340 (M^+).

p-t-Butyl-2-benzoylpyridine 4,4-Dimethyl-3-thiosemicarbazone (t-BuBp44mT). Pale-yellow crystals (yield: 49%). Anal. Calcd for $C_{19}H_{24}N_4S$: C, 66.82; H, 7.38; N, 16.41%. Found: C, 66.78; H, 7.26; N, 16.49%. ^{1}H NMR (DMSO-d_6): 8.84 (d, 1H), 7.99 (td, 1H), 7.58 (td, 1H), 7.53 (d, 2H), 7.45 (d, 2H), 7.34 (d, 1H), 3.31 (s, 3H), 3.09 (s, 3H), 1.31 (s, 9H). MS (EI) m/z 340 (M^+).

p-t-Butyl-2-benzoylpyridine 4-Phenyl-3-thiosemicarbazone (t-BuBBp4pT). Orange crystals (yield: 95%). Anal. Calcd for $C_{23}H_{24}N_4S\cdot 1/2EtOH$: C, 70.04; H, 6.61; N, 13.61%. Found: C, 69.85; H, 7.20; N, 13.59%. ^{1}H NMR (DMSO-d_6): 12.86 (s, 1H), 10.28 (s, 1H), 8.87 (d, 1H), 8.05. (td, 1H), 7.63 (td, 1H), 7.62 (d, 2H), 7.57 (d, 2H), 7.42 (tr, 1H), 7.40 (tr, 2H), 7.37 (d, 1H), 7.27 (d, 2H), 1.31 (s, 9H). MS (EI) m/z 388 (M^+).

General Synthesis of $[Fe^{III}(RBpT)]^+$ Complexes. The iron complexes were prepared by the following general method. The appropriate thiosemicarbazone (3.5 mmol) was dissolved in 10 mL of methanol. Minimal amounts of MeCN were added dropwise to aid dissolution. Once dissolved, 0.36 g of Et_3N was added to the solution. Then, $Fe(ClO_4)_3\cdot 6H_2O$ (0.81 g, 1.7 mmol) was added and the mixture gently refluxed for 60 min. Upon cooling, the dark-brown powder was filtered off and washed with ethanol (10 mL) followed by diethyl ether (10 mL).

$[Fe(MeBpT)_2]ClO_4\cdot CH_3OH$. Yield: 33%. Anal. Calcd for $C_{28}H_{26}ClFeN_8O_4S_2\cdot CH_3OH$: C, 48.0; H, 4.2; N, 15.4%. Found: C, 47.8; H, 4.6; N, 14.7%. IR (cm^{-1}): 3275w, 3102m, 2938w, 2678s, 1620s, 1509s, 1490s, 1430vs, 1325s, 1203s, 1145s, 1119s, 1088s, 941w, 851m,789m, 746m, 653m, 627s. MS (ESI) m/z 694 (M^+).

$[Fe(MeBp4mT)_2]ClO_4$. Yield: 37%. Anal. Calcd for $C_{30}H_{30}ClFeN_8O_4S_2$: C, 49.9; H, 4.2; N, 15.5%. Found: C, 49.5; H, 4.2; N, 15.6%. IR (cm^{-1}): 3386s, 1595w, 1542s, 1521s, 1494s, 1447s, 1397s, 1337s, 1296s, 1269s, 1234s, 1202s, 1164s, 1096vs, 968m, 839w, 812w, 783m, 754m, 623s. MS (ESI) m/z 722 (M^+).

$[Fe(MeBp4eT)_2]ClO_4$. Yield: 38%. Anal. Calcd for $C_{32}H_{34}ClFeN_8O_4S_2$: C, 51.2; H, 4.6; N, 14.9%. Found: C, 51.3; H, 4.7; N, 15.1%. IR (cm^{-1}): 3383w, 1602w, 1543s, 1517s, 1493s, 1427s, 1334s, 1299s, 1266s, 1238s, 1198m, 1160s, 1094vs, 960w, 850m, 834m, 783s, 751w, 625s. MS (ESI) m/z 750 (M^+).

$[Fe(MeBp44mT)_2]ClO_4$. Yield: 39%. Anal. Calcd for $C_{32}H_{34}ClFeN_8O_4S_2$: C, 51.2; H, 4.6; N, 14.9%. Found: C, 50.9; H, 4.6; N, 15.0%. IR (cm^{-1}): 2938w, 1602w, 1543s, 1510s, 1460s, 1437s, 1394s, 1345s, 1302s, 1263s, 1205s, 1154w, 1094vs, 977w, 920s, 783m, 748w, 723m, 692s, 663w, 633w, 620s. MS (ESI) m/z 750 (M^+). Crystals suitable for X-ray work were obtained by slow evaporation of an ethanolic solution of the compound.

$[Fe(MeBp4pT)_2]ClO_4\cdot 1/2H_2O$. Yield: 37%. Anal. Calcd for $C_{40}H_{34}ClFeN_8O_4S_2\cdot 1/2H_2O$: C, 56.2; H, 4.1; N, 13.1%. Found: C, 56.0; H, 4.2; N, 13.3%. IR (cm^{-1}): 3282s, 1600s, 1548s, 1521s, 1492s, 1429vs, 1339s, 1319s, 1254s, 1203w, 1185s, 1119s, 973w, 839w, 814w, 783m, 755s, 693m, 623s. MS (ESI) m/z 846 (M^+).

$[Fe(MeOBpT)_2]ClO_4\cdot H_2O$. Yield: 41%. Anal. Calcd for $C_{28}H_{26}ClFeN_8O_6S_2\cdot H_2O$: C, 45.2; H, 3.8; N, 15.1%. Found: C, 45.4; H, 3.9; N, 14.9%. IR (cm^{-1}): 3434w, 3319m, 3198w, 1604s, 1505s, 1428vs, 1327s, 1251s, 1208s, 1177s, 1152s, 1097vs, 1025s, 953w, 841w, 826w, 784m, 748w, 653m, 624s. MS (ESI) m/z 726 (M^+).

$[Fe(MeOBp4mT)_2]ClO_4$. Yield: 42%. Anal. Calcd for $C_{30}H_{30}ClFeN_8O_6S_2$: C, 47.8; H, 4.0; N, 14.9%. Found: C, 47.6; H, 4.0; N, 14.9%. IR (cm^{-1}): 3381m, 1606s, 1548s, 1522s, 1496s, 1449s, 1401s, 1339m, 1294m, 1253s, 1205m, 1178s, 1085vs, 1031m, 969w, 823w, 782m, 753w, 659w, 624s. MS (ESI) m/z 754 (M^+).

$[Fe(MeOBp4eT)_2]ClO_4\cdot 1/2H_2O$. Yield: 44%. Anal. Calcd for $C_{32}H_{34}ClFeN_8O_6S_2\cdot 1/2H_2O$: C, 48.6; H, 4.5; N, 14.2%. Found: C, 48.4; H, 4.4; N, 14.2%. IR (cm^{-1}): 3618w, 3366w, 2977w, 1602w, 1543s, 1517s, 1493s, 1427s, 1334s, 1299s, 1266s, 1238s, 1198m, 1160s, 1094vs, 960w, 850m, 834m, 783s, 751w, 625s. MS (ESI) m/z 782 (M^+).

$[Fe(MeOBp44mT)_2]ClO_4$. Yield: 31%. Anal. Calcd for $C_{32}H_{34}ClFeN_8O_6S_2$: C, 49.1; H, 4.4; N, 14.3%. Found: C, 49.2; H, 4.5; N, 14.2%. IR (cm^{-1}): 2938w, 1605s, 1548s, 1518s, 1491m, 1454s, 1396s, 1320s, 1304s, 1253vs, 1178s, 1149s, 1092s, 1025m, 968w, 913m, 844w, 820w, 780m, 750w, 624s. MS (ESI) m/z 782 (M^+).

$[Fe(MeOBp4pT)_2]ClO_4\cdot CH_3CN$. Yield: 36%. Anal. Calcd for $C_{40}H_{34}ClFeN_8O_6S_2\cdot CH_3CN$: C, 54.9; H, 4.1; N, 13.7%. Found: C,

dx.doi.org/10.1021/jm301691s | J. Med. Chem. 2013, 56, 357−370

54.5; H, 4.4; N, 13.8%. IR (cm^{-1}): 3059w, 1602s, 1525s, 1496s, 1428vs, 1339s, 1319s, 1251s, 1177s, 1099s, 1027m, 972w, 901w, 833w, 780w, 753s, 693m, 622m. MS (ESI) m/z 878 (M^+).

[Fe(t-BuBpT)$_2$]ClO$_4$·1/2CH$_3$CN. Yield: 40%. Anal. Calcd for $C_{34}H_{40}ClFeN_8O_4S_2$·1/2$CH_3CN$: C, 52.5; H, 5.2; N, 14.9%. Found: C, 52.6; H, 5.4; N, 15.1%. IR (cm^{-1}): 3384w, 3276m, 3148m, 2962m, 2678s, 1619s, 1592m, 1471m, 1425vs, 1344s, 1205m, 1134s, 1083w, 1013w, 943w, 853w, 799w, 782w, 655m, 562m. MS (ESI) m/z 780 (M^+).

[Fe(t-BuBp4mT)$_2$]ClO$_4$·CH$_3$OH. Yield: 42%. Anal. Calcd for $C_{36}H_{44}ClFeN_8O_4S_2$·$CH_3OH$: C, 52.9; H, 5.8; N, 13.3%. Found: C, 52.6; H, 6.0; N, 13.5%. IR (cm^{-1}): 3386s, 1595w, 1542s, 1521s, 1494s, 1447s, 1397s, 1337s, 1296s, 1269s, 1234s, 1202s, 1164s, 1096vs, 968m, 839w, 812w, 783m, 754m, 623s. MS (ESI) m/z 808 (M^+).

[Fe(t-BuBp4eT)$_2$]ClO$_4$·H$_2$O. Yield: 28%. Anal. Calcd for $C_{38}H_{48}ClFeN_8O_4S_2$·$H_2O$: C, 53.4; H, 5.9; N, 13.1%. Found: C, 53.8; H, 6.1; N, 13.0%. IR (cm^{-1}): 3383w, 1602w, 1543s, 1517s, 1493s, 1427s, 1334s, 1299s, 1266s, 1238s, 1198m, 1160s, 1094vs, 960w, 850m, 834m, 783s, 751w, 625s. MS (ESI) m/z 836 (M^+).

[Fe(t-BuBp44mT)$_2$]ClO$_4$. Yield: 38%. Anal. Calcd for $C_{38}H_{48}ClFeN_8O_4S_2$: C, 54.6; H, 5.8; N, 13.4%. Found: C, 54.8; H, 5.7; N, 13.7%. IR (cm^{-1}): 2938w, 1602w, 1543s, 1510s, 1460s, 1437s, 1394s, 1345s, 1302s, 1263s, 1205s, 1154w, 1094vs, 977w, 920s, 783m, 748w, 723m, 692s, 663w, 633w, 620s. MS (ESI) m/z 836 (M^+).

[Fe(t-BuBp4pT)$_2$]ClO$_4$·1/2CH$_3$CN. Yield: 43%. Anal. Calcd for $C_{46}H_{48}ClFeN_8O_4S_2$·1/2$CH_3CN$: C, 59.2; H, 5.2; N, 12.5%. Found: C, 59.6; H, 5.5; N, 12.5%. IR (cm^{-1}): 3282s, 1600s, 1548s, 1521s, 1492s, 1429vs, 1339s, 1319s, 1254s, 1203w, 1185s, 1119s, 973w, 839w, 814w, 783m, 755s, 693m, 623s. MS (ESI) m/z 932 (M^+).

Biological Studies. *Cell Culture.* Chelators were dissolved in DMSO as 10 mM stock solutions and diluted in medium containing 10% fetal calf serum (Commonwealth Serum Laboratories, Melbourne, Australia) so that the final [DMSO] < 0.5% (v/v). At this final concentration, DMSO had no effect on proliferation, ^{59}Fe uptake, or ^{59}Fe mobilization from cells, as shown previously.[24] The human SK-N-MC neuroepithelioma cell line and mortal human MRC5 fibroblasts (American Type Culture Collection, Manassas, VA) were grown by standard procedures[24] at 37 °C in a humidified atmosphere of 5% CO_2/95% air in an incubator (Forma Scientific, Marietta, OH).

Effect of the Chelators on Cellular Proliferation. The effect of the chelators and complexes on cellular proliferation were determined by the [1-(4,5-dimethylthiazol-2-yl)-2,5-diphenyl tetrazolium] (MTT) assay using standard techniques.[24,28,40] The SK-N-MC cell line was seeded in 96-well microtiter plates at 1.5 × 10^4 cells/well in medium containing human $^{56}Fe_2$-Tf (1.25 μM) and chelators or complexes at a range of concentrations (0−25 μM). Control samples contained medium with Fe_2-Tf (1.25 μM) without the ligands. The cells were incubated at 37 °C in a humidified atmosphere containing 5% CO_2 and 95% air for 72 h. After this incubation, 10 μL of MTT (5 mg/mL) was added to each well and further incubated at 37 °C/2 h. After solubilization of the cells with 100 μL of 10% SDS-50% isobutanol in 10 mM HCl, the plates were read at 570 nm using a scanning multiwell spectrophotometer. The inhibitory concentration (IC_{50}) was defined as the chelator concentration necessary to reduce the absorbance to 50% of the untreated control. Using this method, absorbance was shown to be directly proportional to cell counts, as shown previously.[24]

Preparation of ^{56}Fe- and ^{59}Fe-Transferrin. Human Tf (Sigma) was labeled with ^{56}Fe or ^{59}Fe (Dupont NEN, MA) to produce $^{56}Fe_2$-Tf or $^{59}Fe_2$-Tf, respectively, as previously described.[24,25] Unbound ^{59}Fe was removed by passage through a Sephadex G25 column and exhaustive vacuum dialysis against a large excess of 0.15 M NaCl buffered to pH 7.4 with 1.4% $NaHCO_3$ by standard methods.[24,25]

Effect of Chelators on ^{59}Fe Efflux from Cells. Iron efflux experiments examining the ability of various chelators to mobilize ^{59}Fe from SK-N-MC cells were performed using established techniques.[23,24] Briefly, following prelabeling of cells with $^{59}Fe_2$-Tf (0.75 μM) for 3 h/37 °C, the cell cultures were washed on ice four times with ice-cold PBS and then subsequently incubated with each chelator (25 μM) for 3 h/37 °C. The overlying media containing released ^{59}Fe was then separated from the cells using a Pasteur pipet. Radioactivity was measured in both the cell pellet and supernatant using a γ-scintillation counter (Wallac Wizard 3, Turku, Finland). In these studies, the novel ligands were compared to the previously characterized chelators, DFO, NIH, and Dp44mT.

Effect of Chelators at Preventing $^{59}Fe_2$-Tf Uptake from $^{59}Fe_2$-Tf by Cells. The ability of the chelator to prevent cellular ^{59}Fe uptake from the serum Fe transport protein, $^{59}Fe_2$-Tf, was examined using established techniques.[28,56] Briefly, cells were incubated with $^{59}Fe_2$-Tf (0.75 μM) for 3 h/37 °C in the presence of each of the chelators (25 μM). The cells were then washed four times with ice-cold PBS, and internalized ^{59}Fe was determined by standard techniques by incubating the cell monolayer for 30 min/4 °C with the general protease, Pronase (1 mg/mL; Sigma).[28,56] The cells were removed from the monolayer using a plastic spatula and centrifuged at 14000 rpm/1 min. The supernatant represents membrane-bound, Pronase-sensitive ^{59}Fe that was released by the protease, while the Pronase-insensitive fraction represents internalized ^{59}Fe.[24,28,56] The novel ligands were compared to the previously characterized chelators, DFO, NIH, and Dp44mT.

Ascorbate Oxidation Assay. An established protocol was used to measure ascorbate oxidation with the following modification, namely acetonitrile (25% v/v) was added to the buffer to enable dissolution of the lipophilic RBpT chelators.[11,28,57] Briefly, ascorbic acid (100 μM) was prepared immediately prior to an experiment and incubated in the presence of Fe^{III} (10 μM; added as $FeCl_3$), a 50-fold molar excess of citrate (500 μM) and the chelator (1−60 μM). Absorbance at 265 nm was measured after 10 and 40 min at room temperature and the decrease of intensity between these time points calculated.[11,28] The results of these experiments were expressed in terms of iron-binding equivalents (IBE) due to the varying denticity of the chelators examined.

Hemoglobin Preparation. Hemoglobin samples were prepared as previously described.[36] Briefly, blood samples were collected from healthy human donors in Vacutainer collection tubes (BD, Plymouth, UK) and used immediately. RBCs were isolated by centrifugation (480*g*/5 min/4 °C) and then washed in Hank's balanced salt solution (HBSS). RBCs were resuspended 1:1 in HBSS, and incubations using intact RBCs (15% hematocrit) were performed for 3 h/37 °C in the presence and absence of chelators (25 μM). To prepare RBC lysates, RBCs were lysed with ultrapure water, the debris removed by centrifugation (16000*g*/30 min/4 °C), and the supernatant utilized ([oxyHb] = 1.5 mM; from 15% hematocrit content). Again, assays using RBC lysates were performed using a 3 h incubation at 37 °C in the presence and absence of chelators (25 μM).

Spectral Analysis of MetHb. Spectra of MetHb were analyzed as previously described.[36] Spectra (250−700 nm) of RBC lysates were obtained using a Shimadzu UV−vis spectrophotometer (UV-1800; Shimadzu, Kyoto, Japan). Concentrations of oxyHb and metHb were determined at 577 and 630 nm.[50]

Statistical Analysis. Experimental data were compared using Student's *t*-test. Results were expressed as mean ± SD (number of experiments) and considered to be statistically significant when $p < 0.05$.

■ ASSOCIATED CONTENT

Ⓢ Supporting Information

Crystal structures and bond lengths and angles. This material is available free of charge via the Internet at http://pubs.acs.org.

■ AUTHOR INFORMATION

Corresponding Author

*For D.S.K.: phone, +61-2-9036-6547; fax, +61-2-9351-3429; E-mail, danutak@med.usyd.edu.au. For D.R.R.: phone, +61-2-9036-6548; fax, +61-2-9036-6549; E-mail, d.richardson@med.usyd.edu.au.

Notes

The authors declare no competing financial interest.

■ ACKNOWLEDGMENTS

Financial support from the National Health and Medical Research Council (Senior Principal Research Fellowship and Project Grants to D.R.R.) and Australian Research Council (DP0773027 to P.V.B. and D.R.R. and DP1096029 to P.V.B.) is gratefully acknowledged. P.J.J. (10/CDF/2-15) and D.S.K. (08/ECF/1-30) thank the Cancer Institute NSW for Fellowship support. C.S. is the grateful recipient of an Australian Postgraduate Award from the University of Sydney.

■ ABBREVIATIONS USED

3-AP, 3-aminopyridine-2-carboxaldehyde thiosemicarbazone; DFO, desferrioxamine; BpT, 2′-benzoylpyridine thiosemicarbazone; Bp4mT, 2′-benzoylpyridine 4-methyl-3-thiosemicarbazone; Bp4eT, 2′-benzoylpyridine 4-ethyl-3-thiosemicarbazone; Bp44mT, 2′-benzoylpyridine 4,4-dimethyl-3-thiosemicarbazone; DpT, di-2′-pyridylketone thiosemicarbazone; Dp44mT, di-2′-pyridylketone 4,4-dimethyl-3-thiosemicarbazone; IBE, iron-binding equivalent; metHb, methemoglobin; NHE, normal hydrogen electrode; NIH, 2-hydroxy-1-naphthaldehyde isonicotinoyl hydrazone; oxyHb, oxyhemoglobin; RBC, red blood cell; RBpT, 2′-(4″-alkylbenzoyl)pyridine thiosemicarbazone; RBp4mT, 2′-(4″-alkylbenzoyl)pyridine 4-methyl-3-thiosemicarbazone; RBp4eT, 2′-(4″-alkylbenzoyl)pyridine 4-ethyl-3-thiosemicarbazone; RBp44mT, 2′-(4″-alkylbenzoyl)pyridine 4,4-dimethyl-3-thiosemicarbazone; RBp4pT, 2′-(4″-alkylbenzoyl)-pyridine 4-phenyl-3-thiosemicarbazone; ROS, reactive oxygen species; Tf, transferrin

■ REFERENCES

(1) Andrews, N. C. Disorders of Iron Metabolism. *N. Engl. J. Med.* **1999**, *341*, 1986−1995.

(2) Iancu, T. C.; Shiloh, H.; Kedar, A. Neuroblastomas Contain Iron-Rich Ferritin. *Cancer* **1988**, *61*, 2497−2502.

(3) Hoyes, K. P.; Hider, R. C.; Porter, J. B. Cell Cycle Synchronization and Growth Inhibition by 3-Hydroxypyridin-4-one Iron Chelators in Leukemia Cell Lines. *Cancer Res.* **1992**, *52*, 4591−4599.

(4) Le, N. T.; Richardson, D. R. The Role of Iron in Cell Cycle Progression and the Proliferation of Neoplastic Cells. *Biochim. Biophys. Acta* **2002**, *1603*, 31−46.

(5) Larrick, J. W.; Cresswell, P. Modulation of Cell Surface Iron Transferrin Receptors by Cellular Density and State of Activation. *J. Supramol. Struct.* **1979**, *11*, 579−586.

(6) Elford, H. L.; Freese, M.; Passamani, E.; Morris, H. P. Ribonucleotide Reductase and Cell Proliferation. I. Variations of Ribonucleotide Reductase Activity with Tumor Growth Rate in a Series of Rat Hepatomas. *J. Biol. Chem.* **1970**, *245*, 5228−5233.

(7) Cooper, C. E.; Lynagh, G. R.; Hoyes, K. P.; Hider, R. C.; Cammack, R.; Porter, J. B. The Relationship of Intracellular Iron Chelation to the Inhibition and Regeneration of Human Ribonucleotide Reductase. *J. Biol. Chem.* **1996**, *271*, 20291−20299.

(8) Nyholm, S.; Mann, G. J.; Johansson, A. G.; Bergeron, R. J.; Graslund, A.; Thelander, L. Role of Ribonucleotide Reductase in Inhibition of Mammalian Cell Growth by Potent Iron Chelators. *J. Biol. Chem.* **1993**, *268*, 26200−26205.

(9) Blatt, J.; Stitely, S. Antineuroblastoma Activity of Desferoxamine in Human Cell Lines. *Cancer Res.* **1987**, *47*, 1749−1750.

(10) Buss, J. L.; Torti, F. M.; Torti, S. V. The Role of Iron Chelation in Cancer Therapy. *Curr. Med. Chem.* **2003**, *10*, 1021−1034.

(11) Chaston, T. B.; Lovejoy, D. B.; Watts, R. N.; Richardson, D. R. Examination of the Antiproliferative Activity of Iron Chelators: Multiple Cellular Targets and the Different Mechanism of Action of Triapine Compared with Desferrioxamine and the Potent Pyridoxal Isonicotinoyl Hydrazone Analogue 311. *Clin. Cancer Res.* **2003**, *9*, 402−414.

(12) Donfrancesco, A.; Deb, G.; Dominici, C.; Angioni, A.; Caniglia, M.; De Sio, L.; Fidani, P.; Amici, A.; Helson, L. Deferoxamine, Cyclophosphamide, Etoposide, Carboplatin, and Thiotepa (D-CECaT): A New Cytoreductive Chelation-Chemotherapy Regimen in Patients with Advanced Neuroblastoma. *Am. J. Clin. Oncol.* **1992**, *15*, 319−322.

(13) Donfrancesco, A.; Deb, G.; Dominici, C.; Pileggi, D.; Castello, M. A.; Helson, L. Effects of a Single Course of Deferoxamine in Neuroblastoma Patients. *Cancer Res.* **1990**, *50*, 4929−4930.

(14) Estrov, Z.; Tawa, A.; Wang, X. H.; Dube, I. D.; Sulh, H.; Cohen, A.; Gelfand, E. W.; Freedman, M. H. In Vitro and In Vivo Effects of Deferoxamine in Neonatal Acute Leukemia. *Blood* **1987**, *69*, 757−761.

(15) Torti, S. V.; Torti, F. M.; Whitman, S. P.; Brechbiel, M. W.; Park, G.; Planalp, R. P. Tumor Cell Cytotoxicity of a Novel Metal Chelator. *Blood* **1998**, *92*, 1384−1389.

(16) Turner, J.; Koumenis, C.; Kute, T. E.; Planalp, R. P.; Brechbiel, M. W.; Beardsley, D.; Cody, B.; Brown, K. D.; Torti, F. M.; Torti, S. V. Tachpyridine, a Metal Chelator, Induces G2 Cell-Cycle Arrest, Activates Checkpoint Kinases, and Sensitizes Cells to Ionizing Radiation. *Blood* **2005**, *106*, 3191−3199.

(17) Kovacevic, Z.; Kalinowski, D. S.; Lovejoy, D. B.; Yu, Y.; Suryo Rahmanto, Y.; Sharpe, P. C.; Bernhardt, P. V.; Richardson, D. R. The Medicinal Chemistry of Novel Iron Chelators for the Treatment of Cancer. *Curr. Top. Med. Chem.* **2011**, *11*, 483−499.

(18) Yu, Y.; Gutierrez, E.; Kovacevic, Z.; Saletta, F.; Obeidy, P.; Suryo Rahmanto, Y.; Richardson, D. R. Iron Chelators for the Treatment of Cancer. *Curr. Med. Chem.* **2012**, *19*, 2689−2702.

(19) Fu, D.; Richardson, D. R. Iron Chelation and Regulation of the Cell Cycle: 2 Mechanisms of Posttranscriptional Regulation of the Universal Cyclin-Dependent Kinase Inhibitor p21CIP1/WAF1 by Iron Depletion. *Blood* **2007**, *110*, 752−761.

(20) Le, N. T.; Richardson, D. R. Iron Chelators with High Antiproliferative Activity Up-Regulate the Expression of a Growth Inhibitory and Metastasis Suppressor Gene: A Link Between Iron Metabolism and Proliferation. *Blood* **2004**, *104*, 2967−2975.

(21) Nurtjahja-Tjendraputra, E.; Fu, D.; Phang, J. M.; Richardson, D. R. Iron Chelation Regulates Cyclin D1 Expression via the Proteasome: A Link to Iron Deficiency-Mediated Growth Suppression. *Blood* **2007**, *109*, 4045−4054.

(22) Yu, Y.; Kalinowski, D. S.; Kovacevic, Z.; Siafakas, A. R.; Jansson, P. J.; Stefani, C.; Lovejoy, D. B.; Sharpe, P. C.; Bernhardt, P. V.; Richardson, D. R. Thiosemicarbazones from the old to new: iron chelators that are more than just ribonucleotide reductase inhibitors. *J. Med. Chem.* **2009**, *52*, 5271−5294.

(23) Baker, E.; Richardson, D.; Gross, S.; Ponka, P. Evaluation of the Iron Chelation Potential of Hydrazones of Pyridoxal, Salicylaldehyde and 2-Hydroxy-1-naphthylaldehyde Using the Hepatocyte in Culture. *Hepatology* **1992**, *15*, 492−501.

(24) Richardson, D. R.; Tran, E. H.; Ponka, P. The Potential of Iron Chelators of the Pyridoxal Isonicotinoyl Hydrazone Class as Effective Antiproliferative Agents. *Blood* **1995**, *86*, 4295−4306.

(25) Richardson, D. R.; Milnes, K. The Potential of Iron Chelators of the Pyridoxal Isonicotinoyl Hydrazone Class as Effective Antiproliferative Agents II: The Mechanism of Action of Ligands Derived from Salicylaldehyde Benzoyl Hydrazone and 2-Hydroxy-1-naphthylaldehyde Benzoyl Hydrazone. *Blood* **1997**, *89*, 3025−3038.

(26) Finch, R. A.; Liu, M.; Grill, S. P.; Rose, W. C.; Loomis, R.; Vasquez, K. M.; Cheng, Y.; Sartorelli, A. C. Triapine (3-Aminopyridine-2-carboxaldehyde-thiosemicarbazone): A Potent Inhibitor of Ribonucleotide Reductase Activity with Broad Spectrum Antitumor Activity. *Biochem. Pharmacol.* **2000**, *59*, 983−991.

(27) Yu, Y.; Wong, J.; Lovejoy, D. B.; Kalinowski, D. S.; Richardson, D. R. Chelators at the Cancer Coalface: Desferrioxamine to Triapine and Beyond. *Clin. Cancer Res.* **2006**, *12*, 6876−6883.

(28) Richardson, D. R.; Sharpe, P. C.; Lovejoy, D. B.; Senaratne, D.; Kalinowski, D. S.; Islam, M.; Bernhardt, P. V. Dipyridyl Thiosemicarbazone Chelators with Potent and Selective Antitumor Activity

Form Iron Complexes with Redox Activity. *J. Med. Chem.* **2006**, *49*, 6510−6521.
(29) Yuan, J.; Lovejoy, D. B.; Richardson, D. R. Novel Di-2-pyridyl-Derived Iron Chelators with Marked and Selective Antitumor Activity: In Vitro and in Vivo Assessment. *Blood* **2004**, *104*, 1450−1458.
(30) Karp, J. E.; Giles, F. J.; Gojo, I.; Morris, L.; Greer, J.; Johnson, B.; Thein, M.; Sznol, M.; Low, J. A Phase I Study of the Novel Ribonucleotide Reductase Inhibitor 3-Aminopyridine-2-carboxaldehyde Thiosemicarbazone (3-AP, Triapine) in Combination with the Nucleoside Analog Fludarabine for Patients with Refractory Acute Leukemias and Aggressive Myeloproliferative Disorders. *Leuk. Res.* **2008**, *32*, 71−77.
(31) Ma, B.; Goh, B. C.; Tan, E. H.; Lam, K. C.; Soo, R.; Leong, S. S.; Wang, L. Z.; Mo, F.; Chan, A. T.; Zee, B.; Mok, T. A Multicenter Phase II Trial of 3-Aminopyridine-2-Carboxaldehyde Thiosemicarbazone (3-AP, Triapine) and Gemcitabine in Advanced Non-Small-Cell Lung Cancer with Pharmacokinetic Evaluation using Peripheral Blood Mononuclear Cells. *Invest. New Drugs* **2008**, *26*, 169−173.
(32) Mackenzie, M. J.; Saltman, D.; Hirte, H.; Low, J.; Johnson, C.; Pond, G.; Moore, M. J. A Phase II Study of 3-Aminopyridine-2-carboxaldehyde Thiosemicarbazone (3-AP) and Gemcitabine in Advanced Pancreatic Carcinoma. A Trial of the Princess Margaret Hospital Phase II Consortium. *Invest. New Drugs* **2007**, *25*, 553−558.
(33) Knox, J. J.; Hotte, S. J.; Kollmannsberger, C.; Winquist, E.; Fisher, B.; Eisenhauer, E. A. Phase II Study of Triapine in Patients with Metastatic Renal Cell Carcinoma: A Trial of the National Cancer Institute of Canada Clinical Trials Group (NCIC IND.161). *Invest. New Drugs* **2007**, *25*, 471−477.
(34) Traynor, A. M.; Lee, J. W.; Bayer, G. K.; Tate, J. M.; Thomas, S. P.; Mazurczak, M.; Graham, D. L.; Kolesar, J. M.; Schiller, J. H. A Phase II Trial of Triapine (NSC #663249) and Gemcitabine as Second Line Treatment of Advanced Non-Small Cell Lung Cancer: Eastern Cooperative Oncology Group Study 1503. *Invest. New Drugs* **2010**, *28*, 91−97.
(35) Yen, Y.; Margolin, K.; Doroshow, J.; Fishman, M.; Johnson, B.; Clairmont, C.; Sullivan, D.; Sznol, M. A Phase I Trial of 3-Aminopyridine-2-carboxaldehyde Thiosemicarbazone in Combination with Gemcitabine for Patients with Advanced Cancer. *Cancer Chemother. Pharmacol.* **2004**, *54*, 331−342.
(36) Quach, P.; Gutierrez, E.; Basha, M. T.; Kalinowski, D. S.; Sharpe, P. C.; Lovejoy, D. B.; Bernhardt, P. V.; Jansson, P. J.; Richardson, D. R. Methemoglobin Formation by 3-AP, Dp44mT and Other Anti-Cancer Thiosemicarbazones: Identification of Novel Thiosemicarbazones and Therapeutics that Prevent this Effect. *Mol. Pharmacol.* **2012**, *82*, 105−114.
(37) Whitnall, M.; Howard, J.; Ponka, P.; Richardson, D. R. A Class of Iron Chelators with a Wide Spectrum of Potent Antitumor Activity that Overcomes Resistance to Chemotherapeutics. *Proc. Natl. Acad. Sci. U. S. A.* **2006**, *103*, 14901−14906.
(38) Jansson, P. J.; Hawkins, C. L.; Lovejoy, D. B.; Richardson, D. R. The Iron Complex of Dp44mT is Redox-Active and Induces Hydroxyl Radical Formation: An EPR Study. *J. Inorg. Biochem.* **2010**, *104*, 1224−1228.
(39) Bernhardt, P. V.; Sharpe, P. C.; Islam, M.; Lovejoy, D. B.; Kalinowski, D. S.; Richardson, D. R. Iron Chelators of the Dipyridylketone Thiosemicarbazone Class: Precomplexation and Transmetalation Effects on Anticancer Activity. *J. Med. Chem.* **2009**, *52*, 407−415.
(40) Kalinowski, D. S.; Yu, Y.; Sharpe, P. C.; Islam, M.; Liao, Y. T.; Lovejoy, D. B.; Kumar, N.; Bernhardt, P. V.; Richardson, D. R. Design, Synthesis, and Characterization of Novel Iron Chelators: Structure−Activity Relationships of the 2-Benzoylpyridine Thiosemicarbazone Series and their 3-Nitrobenzoyl Analogues as Potent Antitumor Agents. *J. Med. Chem.* **2007**, *50*, 3716−3729.
(41) Yu, Y.; Rahmanto, Y. S.; Richardson, D. R. Bp44mT: An Orally Active Iron Chelator of the Thiosemicarbazone Class with Potent Anti-Tumour Efficacy. *Br. J. Pharmacol.* **2012**, *165*, 148−166.
(42) Richardson, D. R.; Kalinowski, D. S.; Richardson, V.; Sharpe, P. C.; Lovejoy, D. B.; Islam, M.; Bernhardt, P. V. 2-Acetylpyridine Thiosemicarbazones are Potent Iron Chelators and Antiproliferative Agents: Redox Activity, Iron Complexation and Characterization of their Antitumor Activity. *J. Med. Chem.* **2009**, *52*, 1459−1470.
(43) Bernhardt, P. V.; Caldwell, L. M.; Chaston, T. B.; Chin, P.; Richardson, D. R. Cytotoxic Iron Chelators: Characterization of the Structure, Solution Chemistry and Redox Activity of Ligands and Iron Complexes of the Di-2-pyridyl Ketone Isonicotinoyl Hydrazone (HPKIH) Analogues. *J. Biol. Inorg. Chem.* **2003**, *8*, 866−880.
(44) Chaston, T. B.; Watts, R. N.; Yuan, J.; Richardson, D. R. Potent Antitumor Activity of Novel Iron Chelators Derived from Di-2-pyridylketone Isonicotinoyl Hydrazone involves Fenton-Derived Free Radical Generation. *Clin. Cancer Res.* **2004**, *10*, 7365−7374.
(45) Stefani, C.; Punnia-Moorthy, G.; Lovejoy, D. B.; Jansson, P. J.; Kalinowski, D. S.; Sharpe, P. C.; Bernhardt, P. V.; Richardson, D. R. Halogenated 2′-Benzoylpyridine Thiosemicarbazone (XBpT) Chelators with Potent and Selective Anti-Neoplastic Activity: Relationship to Intracellular Redox Activity. *J. Med. Chem.* **2011**, *54*, 6936−6948.
(46) Kalinowski, D. S.; Richardson, D. R. The Evolution of Iron Chelators for the Treatment of Iron Overload Disease and Cancer. *Pharmacol. Rev.* **2005**, *57*, 547−583.
(47) Kalinowski, D. S.; Sharpe, P. C.; Bernhardt, P. V.; Richardson, D. R. Design, Synthesis, and Characterization of New Iron Chelators with Anti-Proliferative Activity: Structure−Activity Relationships of Novel Thiohydrazone Analogues. *J. Med. Chem.* **2007**, *50*, 6212−6225.
(48) Richardson, D. R. Molecular Mechanisms of Iron Uptake by Cells and the Use of Iron Chelators for the Treatment of Cancer. *Curr. Med. Chem.* **2005**, *12*, 2711−2729.
(49) Halliwell, B.; Gutteridge, J. M. Oxygen Free Radicals and Iron in Relation to Biology and Medicine: Some Problems and Concepts. *Arch. Biochem. Biophys.* **1986**, *246*, 501−514.
(50) Winterbourn, C. C.; Carrell, R. W. Oxidation of Human Haemoglobin by Copper. Mechanism and Suggested Role of the Thiol Group of Residue Beta-93. *Biochem. J.* **1977**, *165*, 141−148.
(51) Liu, M. C.; Lin, T. S.; Sartorelli, A. C. Synthesis and Antitumor Activity of Amino Derivatives of Pyridine-2-Carboxaldehyde Thiosemicarbazone. *J. Med. Chem.* **1992**, *35*, 3672−3677.
(52) Ghose, A. K.; Crippen, G. M. Atomic Physicochemical Parameters for Three-Dimensional-Structure-Directed Quantitative Structure−Activity Relationships. 2. Modeling Dispersive and Hydrophobic Interactions. *J. Chem. Inf. Comput. Sci.* **1987**, *27*, 21−35.
(53) Sheldrick, G. A Short History of SHELX. *Acta Crystallogr., Sect. A: Found. Crystallogr* **2008**, *64*, 112−122.
(54) Farrugia, L. J. ORTEP-3 for Windows—A Version of ORTEP-III with a Graphical User Interface (GUI). *J. Appl. Crystallogr.* **1997**, *30*, 565.
(55) Farrugia, L. J. WINGX—An Integrated System of Windows Programs for the Solution, Refinement and Analysis of Single Crystal X-Ray Diffraction Data. *J. Appl. Crystallogr.* **1999**, *32*, 837−838.
(56) Becker, E.; Richardson, D. R. Development of Novel Aroylhydrazone Ligands for Iron Chelation Therapy: 2-Pyridylcarboxaldehyde Isonicotinoyl Hydrazone Analogs. *J. Lab. Clin. Med.* **1999**, *134*, 510−521.
(57) Dean, R. T.; Nicholson, P. The Action of Nine Chelators on Iron-Dependent Radical Damage. *Free Radical Res.* **1994**, *20*, 83−101.